

Final Report
TNW2011-08
Research Project Agreement No. 61-8435

Accelerating Bridge Construction to Reduce Congestion

Olafur Haraldsson, Research Assistant
Marc O. Eberhard, Professor
John F. Stanton, Professor

Department of Civil and Environmental Engineering
University of Washington
Seattle, WA 98195

Michael Berry, Research Assistant Professor
Montana State University

A report prepared for

Transportation Northwest (TransNow)
University of Washington
135 More Hall, Box 352700
Seattle, Washington 98195-2700

January 2011

TECHNICAL REPORT STANDARD TITLE PAGE

1. REPORT NO. TNW2011-08	2. GOVERNMENT ACCESSION NO.	3. RECIPIENT'S CATALOG NO.	
4. TITLE AND SUBTITLE Accelerating Bridge Construction to Reduce Congestion		5. REPORT DATE 5/11	
		6. PERFORMING ORGANIZATION CODE	
7. AUTHOR(S) Marc O. Eberhard, Olafur Haraldsson, John F. Stanton, Michael Berry		8. PERFORMING ORGANIZATION REPORT NO. TNW2011-08	
9. PERFORMING ORGANIZATION NAME AND ADDRESS Transportation Northwest Regional Center X (TransNow) Box 352700, 112 More Hall University of Washington Seattle, WA 98195-2700		10. WORK UNIT NO.	
		11. CONTRACT OR GRANT NO. DTRT07-G-0010	
12. SPONSORING AGENCY NAME AND ADDRESS United States Department of Transportation Office of the Secretary of Transportation 1200 New Jersey Ave, SE Washington, D.C. 20590		13. TYPE OF REPORT AND PERIOD COVERED Final Technical Report	
		14. SPONSORING AGENCY CODE	
15. SUPPLEMENTARY NOTES			
<p>ABSTRACT</p> <p>The magnitude of the "residual" displacements at the end of an earthquake can affect the amount of time needed to restore a bridge to service. It may be possible to reduce these displacements (and downtimes) by introducing prestressing forces into bridge columns. However, before such systems can be designed, it is necessary to be able to estimate the residual displacements with analytical models. The accuracy of the numerical models needed to be established.</p> <p>In this study, tests of sixteen reinforced concrete columns provided the opportunity to observe experimental trends in residual displacements, and to evaluate the ability of a modeling methodology proposed by Berry and Eberhard (2007) to reproduce the observed behavior. Since the columns were subjected to cyclic loading with imposed displacements rather than an actual earthquake, it was not possible to extract a true residual displacement from the test data. Instead, the results are expressed in terms of cross-over displacements, which are the displacements when the applied effective force is equal to 10% of the effective yield force. The test results indicate that the normalized cross-over ratio (cross-over displacement divided by peak cycle displacement) increases with increasing drift ratio. The normalized cross-over ratio decreases with (a) increases in span-to-depth ratio, (b) decreases in reinforcement ratio, (c) increases in axial-load ratio, and (d) increases in the re-centering ratio. (The re-centering ratio defines the relative quantities of post-tensioned and mild steel reinforcement. As the name implies, it influences the extent to which the column re-centers when the lateral load is removed). The model did reproduce the expected trends in span-to-depth ratio, axial-load ratio and re-centering ratio, but it did not reproduce the observed trend in longitudinal reinforcement ratio. The corresponding analytical estimates of the cross-over ratios consistently exceeded the measured displacements by approximately 20%.</p>			
17. KEY WORDS Key words: bridge, earthquake, precast concrete, pre-tensioning, column, displacement		18. DISTRIBUTION STATEMENT No restrictions. This document is available to the public through the National Technical Information Service, Springfield, VA 22616	
19. SECURITY CLASSIF. (of this report) None	20. SECURITY CLASSIF. (of this page) None	21. NO. OF PAGES 48	22. PRICE

DISCLAIMER

The contents of this report reflect the views of the authors, who are responsible for the facts and the accuracy of the information presented herein. This document disseminated through the Transportation Northwest (TransNow) Regional University Transportation Center under the sponsorship of the Department of Transportation University Transportation Centers Program and through the Washington State Department of Transportation, in the interest of information exchange. The U.S. Government assumes no liability for the contents or use thereof.

CONTENTS

CHAPTER 1: INTRODUCTION.....	1
CHAPTER 2: BACKGROUND	3
2.1 Rapid Construction of Bents in Seismic Regions	3
2.2 Reducing Residual Displacements with Prestressing	3
CHAPTER 3: PROBLEM STATEMENT AND RESEARCH OBJECTIVES.	7
CHAPTER 4: METHOD OF ANALYSIS.....	8
4.1 Column Test Data	8
4.2 Analytical Model	11
CHAPTER 5: RESULTS	13
5.1 Trends in Experimental Data	13
5.2 Accuracy of Simulations.....	18
5.3 Parametric Study with Analytical Model.....	21
CHAPTER 6: CONCLUSIONS AND RECOMMENDATIONS.....	24
6.1 Conclusions.....	24
6.2 Recommendations.....	24
REFERENCES.....	26
APPENDIX A. MEASURED AND CALCULATED EFFECTIVE FORCE – DRIFT RATIO HYSTERETIC RELATIONSHIPS.....	28
APPENDIX B. MEASURED AND CALCULATED NORMALIZED CROSS- OVER DISPLACMENT VERSUS PEAK DRIFT RATIO	37

CHAPTER 1: INTRODUCTION

Bridge construction activities in urban regions exacerbate traffic congestion, which in turn increases fuel consumption and greenhouse emissions. Prefabrication of bridge elements has the potential to accelerate the bridge construction process, which would not only decrease congestion and emissions, but also improve worker safety and bridge quality.

With the support of the Washington State Department of Transportation (WSDOT) and the Federal Highway Research Administration (FHWA) Highways for Life (HFL) program, we have developed a new precast system for constructing bridge bents in seismically active regions. In this system, an easy-to-construct “large-bar, large-duct” detail connects the precast columns to the precast cross-beam (Pang et al. 2010, Steuck et al. 2009). The columns are connected to the supporting cast-in-place footing or drilled shaft using a socket detail. WSDOT will deploy this technology in a bridge spanning over I-5 in 2011.

With the earlier support of TRANSNOW, we tested an enhanced version of the precast bent system, in which a prestressed, post-tensioned element embedded in the column provided a restoring force to reduce post-earthquake residual displacements (Cohagen et al. 2008). Controlling such displacements is critical to returning a bridge to service soon after an earthquake. The tests demonstrated that such columns would perform well during earthquakes, but by themselves, the pseudo-static tests of three isolated columns do not predict the magnitudes of displacements of full bridge systems at the end of an earthquake. To use this technology in practice, it is necessary to reliably predict post-earthquake displacements with analytical models.

This project evaluates the ability of an analytical strategy (OpenSEES, 2010) to predict the response of bridge columns measured in experiments. The real interest lies in residual displacements resulting from true dynamic loading. However, the great majority of tests are cyclic rather than dynamic, and displacement-controlled rather than load-controlled. It is therefore not possible to obtain true post-earthquake residual displacements from them directly.

What can be obtained is the displacement at which the lateral load drops to zero after returning from the peak displacement, and this may be viewed as the static equivalent of the desired dynamic residual displacement. However, after the column undergoes a major displacement excursion, its stiffness near zero load is typically low, with the consequence that the measured zero-load displacement is subject to significant random variation. For this reason, the measured displacement at a low load (10% of the yield load) was used as the target value instead. It gave much more stable results.

CHAPTER 2: BACKGROUND

2.1 RAPID CONSTRUCTION OF BENTS IN SEISMIC REGIONS

If the nation continues to follow traditional construction practices, construction-induced congestion in urban areas will worsen as traffic volumes rise and the number bridge construction sites increases. Until we completed our recent work (Pang et al. 2008a, 2008b, 2008c), no system existed for building bridge bents rapidly in seismically active regions.

Prefabricating bridge bent components offsite reduces the time spent on site, which determines the extent of the interruption to traffic, the fuel wasted by delays, the resulting greenhouse emissions and the public's support for the agency sponsoring the construction. In some cases a component may be erected in such a short time that a "rolling slowdown," rather than a complete lane or roadway closure, is feasible. This option has the huge benefit of eliminating the need to stop traffic. Worker safety is also improved by moving construction activities away from traffic.

With support from the Washington State Department of Transportation, the National Science Foundation, the Pacific Earthquake Engineering Research Center (PEER), and the FHWA Highways for Life program, we developed a rapidly constructible system that connects precast bent columns and beams using a small number of large bars (e.g., #14 or #18) that are grouted into even larger ducts (e.g., 6-in. or 8-in. dia.). Aligning the bars and ducts on site is much easier if the bars are few and the ducts are large. A typical implementation of the concept is shown in Figure 2.1.

Our research showed that this system has similar seismic resistance to conventional cast-in-place construction, but it would be much faster to construct (Pang et al. 2008a, b, c and d). This project was so successful that WSDOT plans on deploying this technology on a bridge (South of Olympia) over I-5 in 2011.

2.2 REDUCING RESIDUAL DISPLACEMENTS WITH PRESTRESSING

An earlier TransNOW project extended our previous research in this area to develop a rapidly constructible bridge bent system that will not only survive a strong earthquake but will also return the bridge to service quickly following the event. With

the support of TransNOW, we tested a system that will likely decrease the residual displacements at the end of the earthquake, thus shortening the likely closure time. This “Hybrid” system depends on using a combination of unbonded post-tensioned tendons and bonded mild steel reinforcement (‘rebar’) to provide the structure’s resistance to seismic loads.

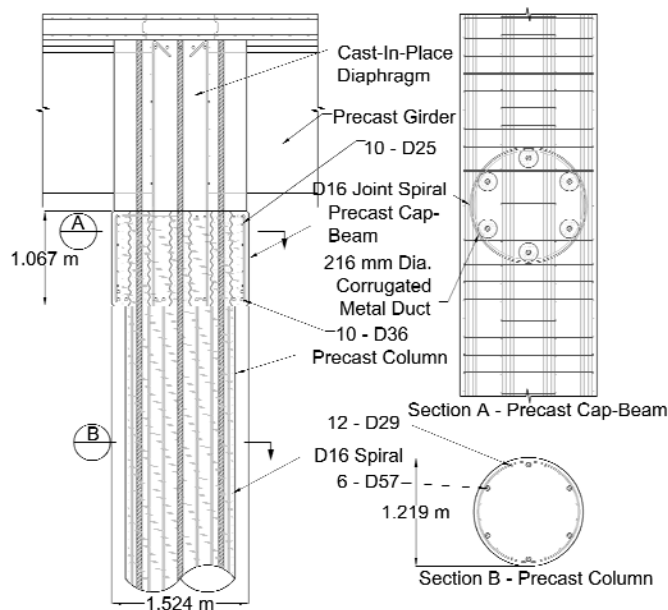


Figure 2.1. Typical Implementation of Precast System

Figure 2.2 shows conceptually the Hybrid Frame concept applied to a bridge bent. The precast concrete column is reinforced with conventional reinforcing bars and an unbonded prestressing tendon. Several methods of making the top and bottom connection are possible, but all result in essentially the same seismic behavior. The system shown in Figure 2.2 consists of reinforcing bars extending from the footing and grouted into ducts in the column, and bars extending from the top of the column into grouted ducts in the cap beam. The post-tensioning tendon is anchored at the bottom of the footing and the top of the cap beam. When the bent is subjected to lateral seismic load, a crack opens at the interface between the column and beam (and another between the column and foundation), so that all the deformations are concentrated there. The bar steel is bonded to the concrete at the cracks, so it undergoes significant extension and yields. The prestressing tendon also stretches but, because it is unbonded, the deformation is spread

over the length of the column, the change in strain is small and it remains elastic. It therefore behaves like a large rubber band, and pulls the column back upright. The system behaves somewhat like the suspension in an automobile: the cyclically yielding bar steel dissipates energy to damp the motion during the earthquake while the tendon acts like a spring to re-center the system when the ground motion stops.

Cohagen et al. (2008) tested isolated columns with post-tensioning. As shown in Figure 2.3, the amount of column deformation at each level of damage was similar for the two hybrid columns (LB6-PT and LB7-PT) as to the column built only with mild reinforcement (LB8). The tests also provided valuable data on the details of the force-displacement hysteresis relationships.

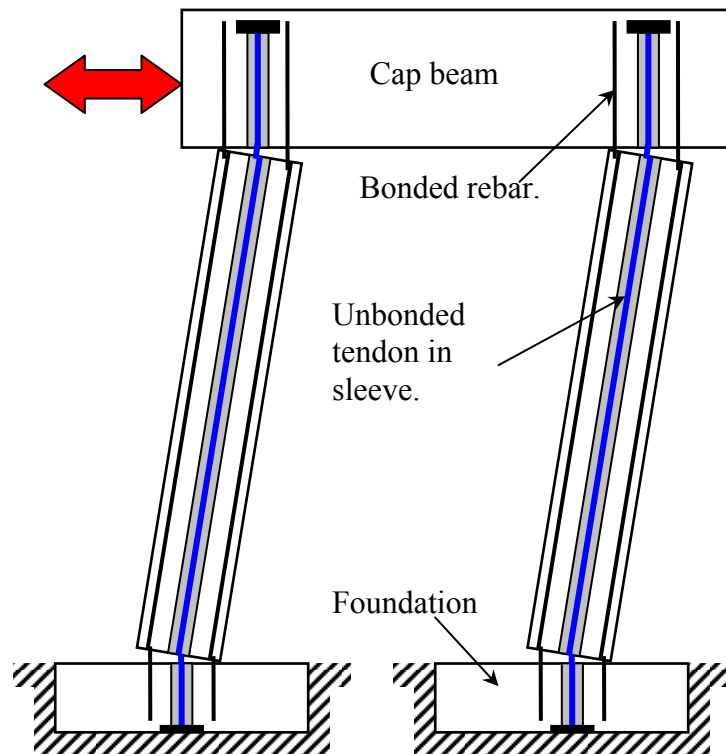


Figure 2.2. Hybrid Frame

However, the test results by themselves do not allow one to predict post-earthquake displacements of bridges, because the tests were static (and earthquakes are dynamic), and because a bridge system is more complicated than an isolated column.

Analytical models are needed to model the dynamic seismic behavior in order for bridge agencies to determine whether the added performance justifies the added investment.

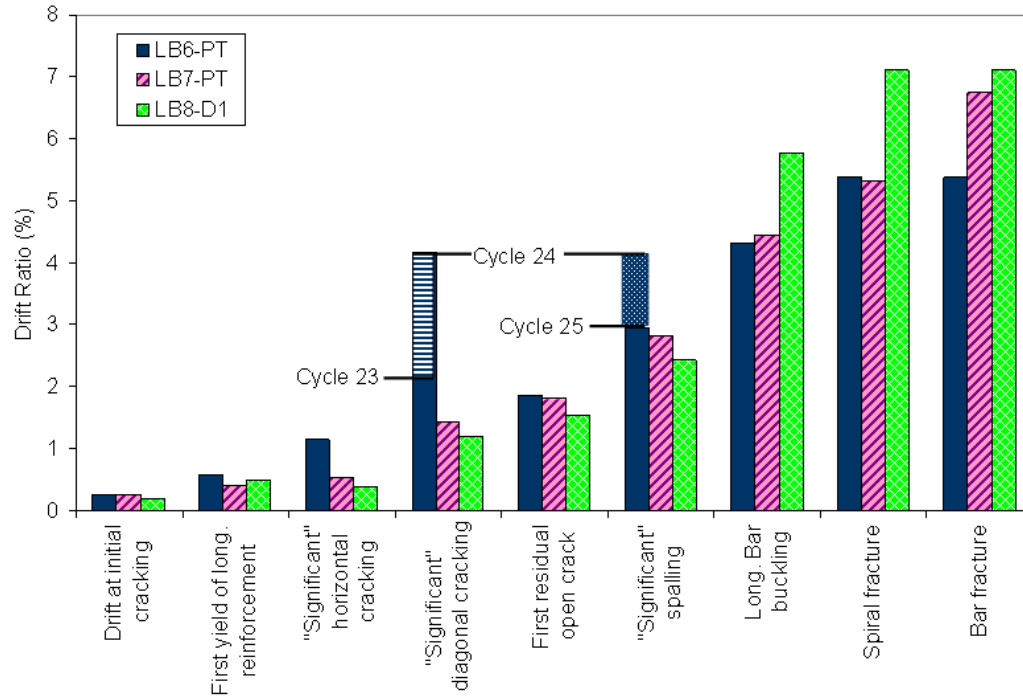


Figure 2.3. Damage Development in Columns with and without Prestressing

CHAPTER 3: PROBLEM STATEMENT AND RESEARCH OBJECTIVES

Berry and Eberhard (2007) developed a detailed model of conventional reinforced concrete columns using the modeling software OpenSEES. Their modeling recommendations lead to analytical models that perform much better than previous models in predicting the force-displacement response of conventional columns at large displacements.

But the accuracy of this methodology has not been evaluated for predicting response at low levels of force that, during an earthquake, would follow large displacement excursions. This low-force behavior needs to be modeled accurately to successfully predict post-earthquake residual displacements. For the purpose of this research, the low-level response is measured by the “cross-over displacement”. Ideally, this would be the displacement at which the force passes through zero following an excursion to a large displacement. In practice, it was found necessary to use the displacement at a small, non-zero force, and 10% of the initial yield force was chosen for the purpose. The accuracy of estimates of the cross-over displacement needs to be evaluated both for conventional columns and for columns that include prestressing.

The objectives of this project are:

1. To identify from the experimental data the key column properties that affect the magnitude of the cross-over displacements.
2. To evaluate the accuracy of the Berry and Eberhard modeling technology in reproducing the experimentally observed cross-over behavior.

Such evaluations are needed to determine whether bridge designers can have confidence in models that predict residual displacements. Such predictions are needed for bridge designers to assess the benefits of implementing the hybrid technology into the new rapid-construction bent system. Such an implementation would reduce traffic congestion and the resulting environmental consequences.

Follow-up studies can then compare the calculated results with the results of the few shake-table tests that are available for comparison.

CHAPTER 4: METHODS OF ANALYSIS

The project included several steps.

1. Identify key trends in experimental data for reinforced concrete columns. The dataset is described in Section 4.1.
2. Evaluate the accuracy of the Berry and Eberhard (2007) modeling strategy in predicting cross-over displacements for conventional and post-tensioned reinforced concrete columns. The modeling strategy is described in Section 4.2.
3. Parametric study of the effect of the key column properties.

4.1 COLUMN TEST DATA

The experimental data used in this study was extracted from the UW-PEER column performance database (Berry et al. 2004). This database provides digital force-displacement histories for column tests, along with the material and geometric properties needed to assemble analytical models.

Key properties for the sixteen tests selected for this study are listed in Table 4.1. In this table, P is the axial load, A_g is the cross-sectional area, f'_c is the concrete compressive strength, ρ_s is the transverse reinforcement ratio, f_{ys} is the yield stress of the spiral reinforcement, ρ_l is the longitudinal reinforcement ratio, and D is the diameter of the column. The effective transverse reinforcement ratio is defined as $\rho_{eff} = \rho_s * f_{ys} / f'_c$.

The sixteen tests were selected for the following reasons.

- Lehman and Moehle (2000) and Calderone et al. (2000) document the results of tests of eight columns. These columns were selected because Berry and Eberhard (2007) previously used them to develop their modeling methodology. They include large variations in the column span-to-depth ratio ($L/D = 4, 8, 10$) with constant level of axial load ($P/A_g f'_c = 7\%$) and longitudinal reinforcement ratio ($\rho_l = 1.5\%$). The tests also include variations in the amount of longitudinal reinforcement ($\rho_l = 0.8, 1.5, 3.0\%$) with constant L/D and axial load.
- Cheok and Stone (1989) and Kowalsky et al. (1999) provided data for columns with higher levels of axial load ($P/A_g f'_c = 21\%$ and 30% , respectively)

- Pang et al. (2008) provided data for a reference cast-in-place concrete column, as well as three precast columns with large bars and large ducts, for various bond conditions.
- Cohagen et al. (2008) provides the data to calibrate a detailed analytical model of the response of a column with both mild steel and post-tensioning.

Table 4.1. Key Properties for Column Tests¹

Reference	Designation	L (mm)	L/D	P _{eff}	P/Agf _c	ρ _l
Lehman and Moehle (2000)	No. 407	2438	4	0.14	0.07	0.008
Lehman and Moehle (2000)	No. 415	2438	4	0.14	0.07	0.015
Lehman and Moehle (2000)	No. 430	2438	4	0.14	0.07	0.03
Lehman and Moehle (2000)	No. 815	4877	8	0.14	0.07	0.015
Lehman and Moehle (2000)	No. 1015	6096	10	0.14	0.07	0.015
Calderone et al. (2000)	No. 328	1829	3	0.16	0.09	0.027
Calderone et al. (2000)	No. 828	4877	8	0.16	0.09	0.027
Calderone et al. (2000)	No. 1028	6096	10	0.16	0.09	0.027
Cheek and Stone (1989)	N2	750	3	0.27	0.21	0.020
Kowalsky et al. (1999)	FL3	3656	8	0.12	0.30	0.036
Pang et al. (2008c)	DB5-RE	1524	3	0.07	0.11	0.016
Pang et al. (2008c)	LB8-FB	1524	3	0.07	0.08	0.015
Pang et al. (2008c)	LB8-D1	1524	3	0.07	0.11	0.015
Pang et al. (2008c)	LB8-D2	1524	3	0.07	0.12	0.015
Cohagen et al. (2008)	LB7-PT	1524	3	0.07	0.13	0.012
Cohagen et al. (2008)	LB6-PT	1524	3	0.07	0.13	0.008

For each test cycle, the cross-over displacement was calculated as shown in Figure 4.1. For both the positive and negative displacements, the displacements ($\Delta_{\text{Cross}1}$, $\Delta_{\text{Cross}2}$) were identified as the displacement corresponding $0.1F_y$ following excursions to larger displacements ($\Delta_{\text{Peak}1}$, $\Delta_{\text{Peak}2}$). The normalized cross-over displacement was then calculated as the ratio of $(\Delta_{\text{Cross}1} - \Delta_{\text{Cross}2}) / (\Delta_{\text{Peak}1} - \Delta_{\text{Peak}2})$.

Cross-over displacements were computed only for cycles in which the peak displacement exceeded the effective yield displacement. The effective yield displacement was defined as follows: (initial yield displacement)* M_n/M_y , where M_y is the moment at first yield, and M_n at is the moment at which the extreme concrete strain was 0.004.

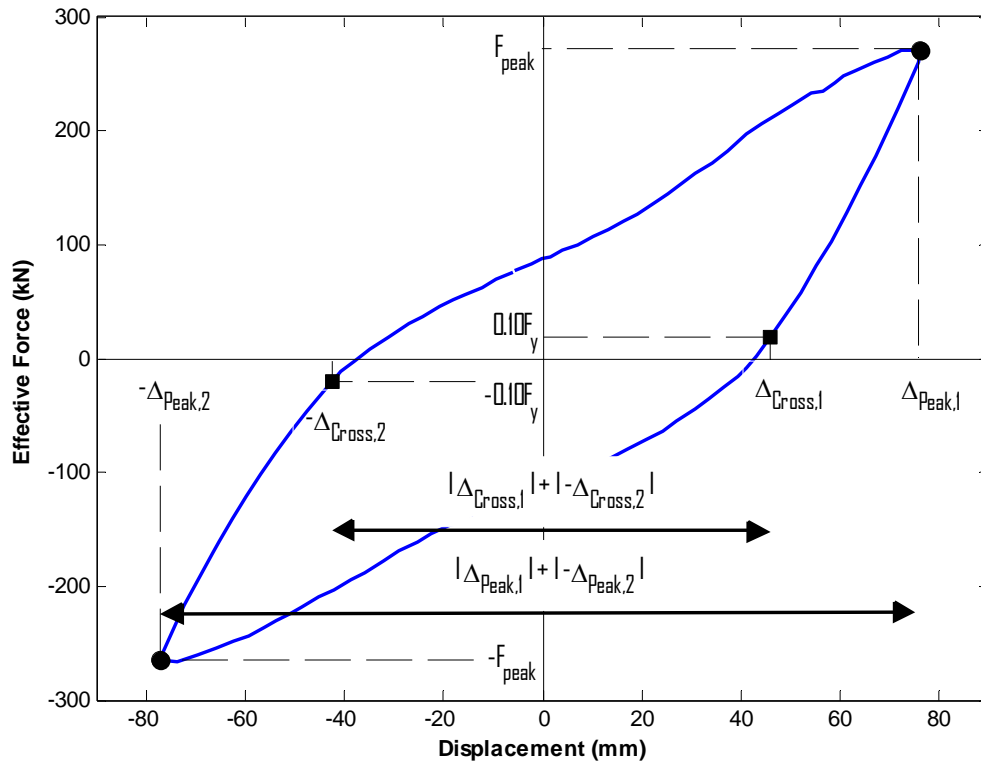


Figure 4.1. Explanation of terms used to calculate the cross-over displacement

4.2 ANALYTICAL MODEL

Berry and Eberhard (2007) developed and calibrated spread-plasticity and lumped-plasticity modeling strategies for columns. The analytical platform OpenSees (2010) was used for this work. This programming environment is attractive, because it is capable of modeling cyclic and bidirectional loading, and variable axial loads.

The spread plasticity, force-based fiber-beam column element is susceptible to strain localization and loss of objectivity in degrading members. So, for the purpose of this study, their lumped-plasticity model formulation was adopted. The following model description is adapted from Berry and Eberhard (2007)

Figure 4.2 shows a typical cantilever column subjected to a lateral load. The figure also shows the moment and actual curvature distributions, and the idealized curvature distributions that are the basis of lumped-plasticity models.

d 2007)

The formulation of the plastic-hinge models employed in design uses the idealized distribution shown in Figure 4.2(d) to develop an expression for the post-yield displacement at the top of the column. In these design models, the curvature is assumed to be linear above the plastic hinge and constant over the height of the plastic hinge.

Scott and Fenves (2006) developed a lumped-plasticity formulation suitable for implementation in a standard displacement-based finite-element environment. The formulation utilizes the force-based fiber beam-column element formulation, and introduces a modified integration scheme, in which inelastic deformations are confined to

an assigned plastic hinge length. This formulation, which is available in OpenSees, results in the curvature distribution shown in Figure 4.2(e). The curvature distribution is linear above the plastic hinge, and within the plastic hinge, the curvature is calculated with moment-curvature analysis.

Berry and Eberhard (2007) discuss the modeling decisions in detail. Computing the tip displacement with a lumped-plasticity model requires computing the moment-curvature response of the column cross-section, estimating the yield displacement, and selecting the plastic-hinge length. The moment-curvature response was computed with a fiber model, using the concrete material object with degraded linear unloading/reloading stiffness (Concrete04), and the Kunnath steel model.

The yield displacement, Δ_y , was calculated using Equation (4.1)

$$\Delta_y = \frac{1}{\alpha_{sec}} \frac{F_y L^3}{3(EI)_{sec}} \quad (4.1)$$

where EI_{sec} is the secant stiffness of the moment-curvature relationship up to the yield moment. F_y is the force at yield, and L is length of the column cantilever. The stiffness modification ratio, α_{sec} , takes into account shear deformation, anchorage slip, and axial load (cracking). This ratio (Berry and Eberhard 2007) was calculated as follows:

$$\alpha_{sec} = 0.35 + 0.1 \frac{L}{D} \leq 1.0 \quad (4.2)$$

The plastic hinge length (Berry and Eberhard 2007) was taken as:

$$L_p = 0.05L + 0.1 \frac{f_y d_b}{\sqrt{f'_c}} \leq \frac{L}{4} \quad (4.3)$$

where f_y , d_b , and f'_c are the yield stress, bar diameter of the tension reinforcement, and concrete strength, respectively.

Within OpenSEES, the plastic hinge analysis was implemented using the `beamWithHinges3` command. This element has two stiffnesses. The pre-yield stiffness in the plastic hinge is determined from the fiber element assigned to it, and the stiffness of the elastic portion is defined by the user's inputs. To obtain the appropriate analytical stiffness for the full column, the elastic stiffness was modified (Berry and Eberhard 2007) in OpenSEES using Equation 4.4.

$$\widehat{\alpha}_{sec} = \frac{\alpha_{sec}(L-L_p)}{L-3\alpha_{sec}L_p} \quad (4.4)$$

CHAPTER 5: RESULTS

This chapter presents the results of our evaluation of the experimental data (Section 5.1), of the simulations of the experimental response (Section 5.2) and of a parametric study using one column (Section 5.3).

5.1 TRENDS IN EXPERIMENTAL DATA

Measured values of cross-over displacements were first obtained from the test data. They were needed as target measurements against which to compare the values predicted by the OpenSEES analytical model. Sets of cross-over displacements were obtained for all sixteen column tests, as described in Section 4.1. In this section, the normalized cross-over displacements (normalized by the peak cycle displacement) are plotted against the peak drift ratio for sets of similar columns, and the influence on response of various column parameters is evaluated.

SPAN-TO-DEPTH RATIO: Figure 5.1 compares the normalized cross-over displacements for tests with three values of the span-to-depth ratio ($L/D = 4, 8$ and 10). All three column tests had the same axial-load ratio (7%), longitudinal reinforcement

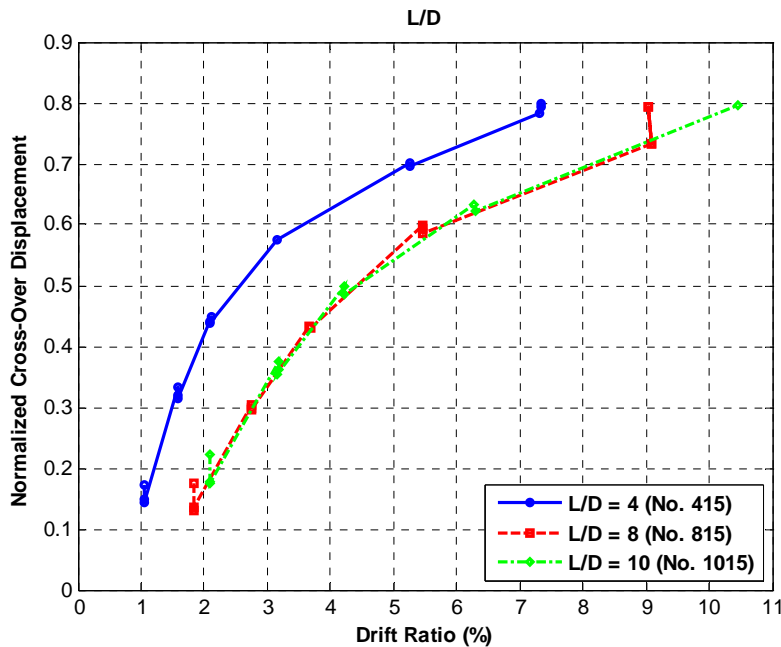


Figure 5.1. Comparison of normalized cross-over displacement vs. peak ratio for different L/D ratios

ratio (1.5%) and effective transverse reinforcement ratio (14%), which is defined as the transverse reinforcement ratio multiplied by the yield strength of the transverse reinforcement and divided by the nominal compressive strength of the concrete. The normalized cross-over displacement at a particular drift ratio was consistently higher for the stockier column ($L/D = 4$) than for the two more slender columns. This observation is consistent with fact that the drift ratio at first yield increases approximately linearly with the span-to-depth ratio, as follows:

$$\frac{\Delta_y}{L} = \frac{1}{\alpha_{sec}} \frac{M_y L}{3(EI)_{sec}} \quad (5.1)$$

REINFORCEMENT RATIO: Figure 5.2 shows the normalized cross-over displacements for three similar columns (similar axial loads, transverse reinforcement and span-to-depth ratios) but with varying longitudinal reinforcement ratios (0.8%, 1.5%, 3.0%). There is little difference between the response of columns with the low and medium reinforcement ratios of 0.8% and 1.5%, but the column with the highest reinforcing ratio (3%) had cross-over displacements that were about 20% lower than that of the less heavily reinforced columns.

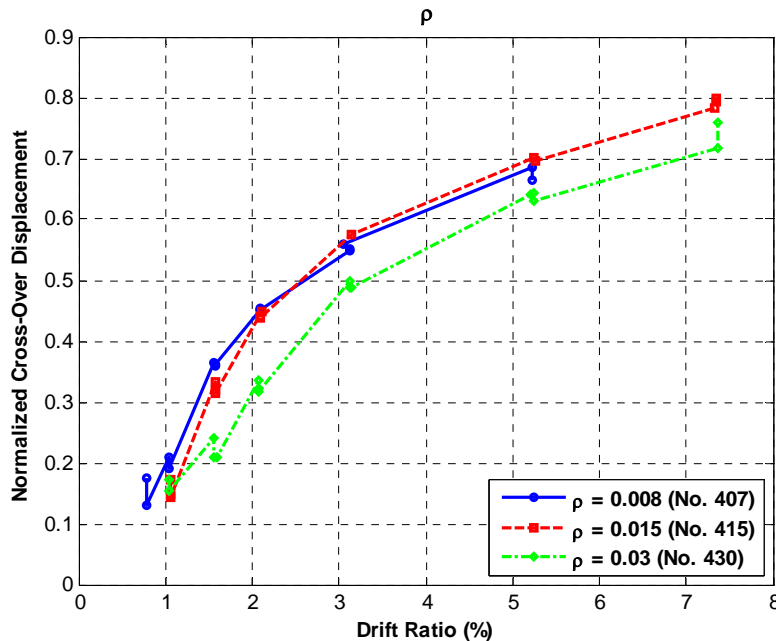


Figure 5.2. Comparison of normalized cross-over displacement vs. peak ratio for different ρ values

This result is consistent with the form of the re-centering ratio, λ_{re} (Cohagen et al. 2008), defined by Equation 5.2.

$$\lambda_{re} = \frac{P_{col} + A_p f_{po}}{A_s f_y} \quad (5.2)$$

where P_{col} is the column axial force, $A_p f_{po}$ is the initial prestressing force, and $A_s f_y$ is the product of the area of the longitudinal reinforcement and the reinforcement yield stress. This ratio compares the magnitudes of forces that tend to make the column re-center (e.g., P_{col} , $A_p f_{po}$) with those (e.g., $A_s f_y$) that tend to resist the re-centering. The smaller cross-over displacements for the column with the most longitudinal reinforcement is consistent with the fact that $A_s f_y$ is larger too.

AXIAL-LOAD RATIO: Figure 5.3 shows the normalized cross-over displacements for two columns with the same span-to-depth ratio ($L/D=3$) but different axial-load ratios (9% and 21%). Similarly, Figure 5.4 shows the normalized cross-over displacements for two columns that are more slender (both have $L/D=8$) but again, have different axial-load ratios (9% and 30%). For both sets of data, the columns with the higher levels of axial load consistently had lower levels of residual displacement. These trends are consistent with Eq. 5.2, in which the column axial load appears in the numerator.

BOND CONDITIONS: Figure 5.5 plots the normalized cross-over displacement for a cast-in-place reference column, as well as three large-bar, large-duct, precast specimens (Pang et al 2008c). The longitudinal reinforcement in one of the specimens was fully bonded to the surrounding grout, whereas in the other two columns, the reinforcement was debonded over a short length. The figure shows that all four columns had nearly identical cross-over displacements.

RE-CENTERING RATIO. Figure 5.6 shows the variation of the cross-over displacement as a function of the re-centering ratio, λ_{re} (Cohagen et al. 2008). Pang's column LB8-D1 had a re-centering ratio of 0.91. Cohagen increased this ratio by reducing the amount of longitudinal mild reinforcement and varying the amount of axial load and prestressing force to obtain ratios of 1.20 and 1.58. The figure shows that the normalized cross-over displacement decreases with increasing re-centering ratio, as expected.

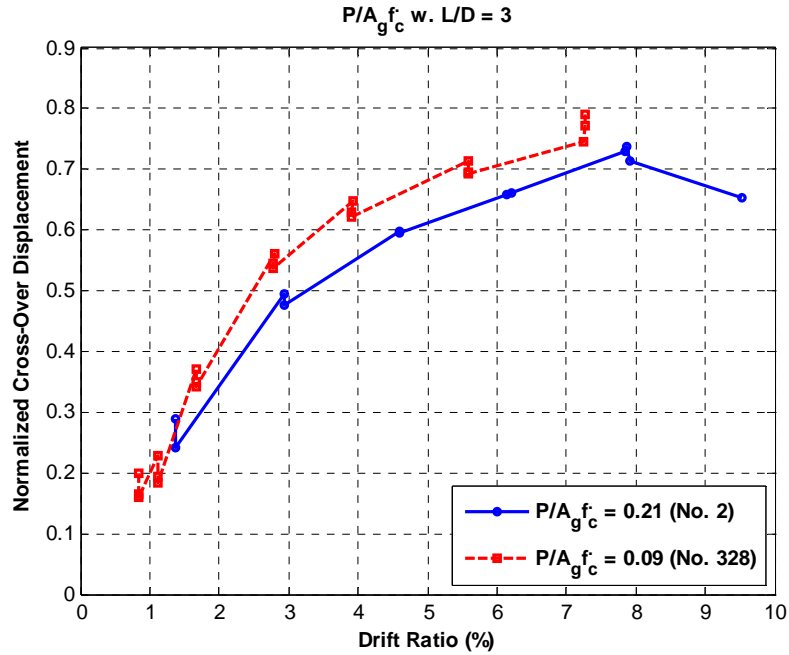


Figure 5.3. Comparison of normalized cross-over displacement vs. peak drift ratio for two values of $P/A_g f_c$ ($L/D=3$)

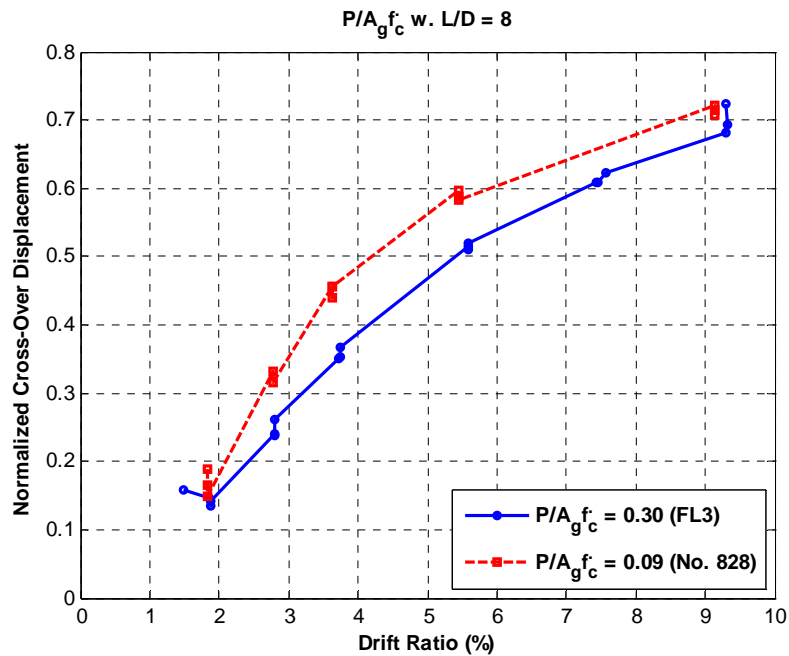


Figure 5.4. Comparison of normalized cross-over displacement vs. peak drift ratio for two values of $P/A_g f_c$ ($L/D = 8$)

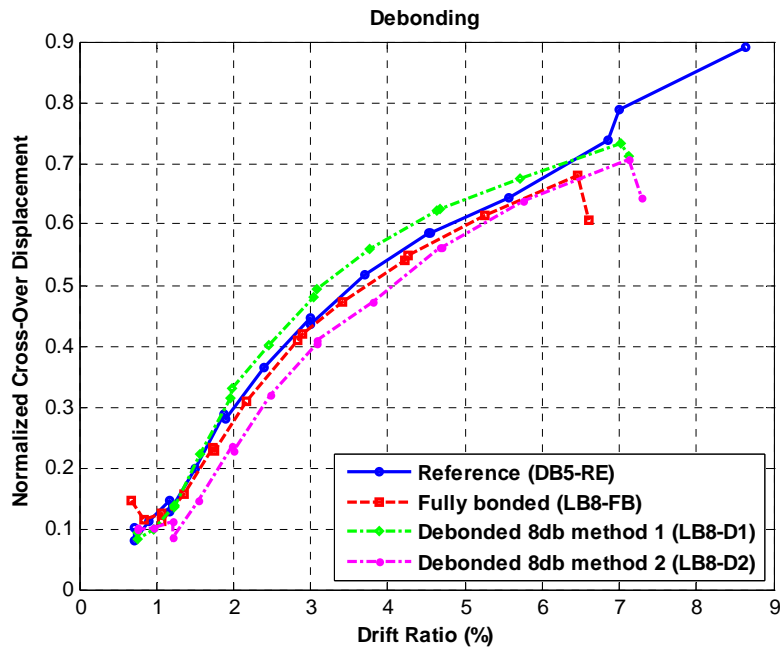


Figure 5.5. Comparison of normalized cross-over displacement vs. peak drift ratio for varying bond conditions between column and cap-beam

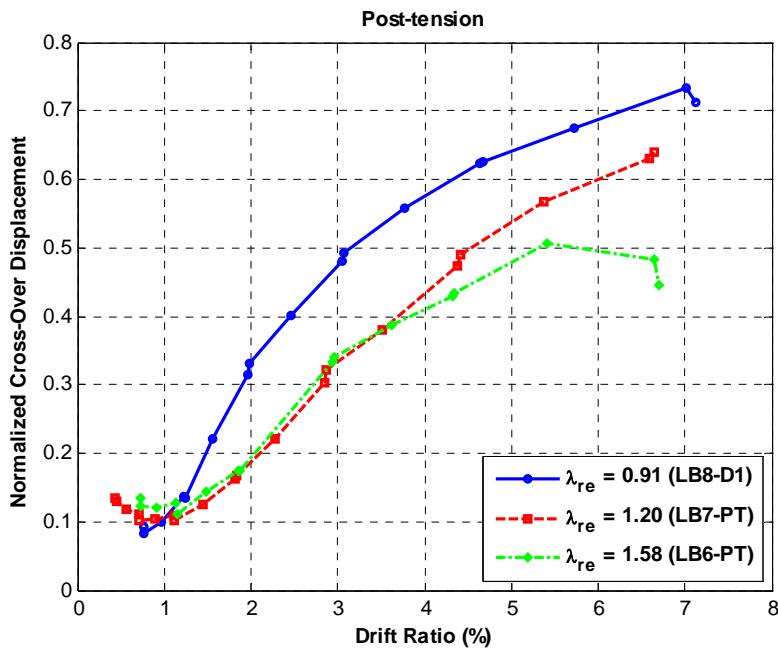


Figure 5.6. Comparison of normalized cross-over displacement vs. peak drift ratio for various re-centering ratios, λ_{re}

5.2 ACCURACY OF SIMULATIONS

Numerical simulations were run for all 16 test columns using the OpenSEES model. The measured and predicted value for the effective yield displacements are compared in Table 5.1 as a measure of the accuracy of the numerical model. The average error is 14%.

Table 5.1. Calculated and Effective Yield Displacements

Column	Predicted Yield Force (kN)	Predicted Effective Yield Displacement (mm)	Measured Effective Yield Displacement (mm)	Relative Error in Displacement (%)
No. 407	133.4	20.7	20.3	+2.0
No. 415	190.4	23	23.4	-1.7
No. 430	307.0	24.48	25.4	-3.6
No. 815	95.2	70.1	83.8	-16.3
No. 1015	76.5	107.1	116.8	-8.3
No. 328	391.5	15.1	14.5	+4.1
No. 828	146.8	69.4	87.1	-20.3
No. 1028	117.4	108.1	133.4	-19.0
N2	57.96	7.28	NA	-
FL3	136.1	49.6	NA	-
DB5-RE	218.1	11.8	9.4	+25.5
LB8-FB	231.2	11.2	NA	-
LB8-D1	248.6	11.4	NA	-
LB8-D2	233.3	11.9	8.82	+34.9
LB7-PT	213.2	6.3	7.0	-10.0
LB6-PT	205.8	11.8	9.8	+20.4

The measured and calculated force-displacement hysteresis curves for all 16 tests are provided in Appendix A. Figure 5.7, reproduced from this appendix, compares the measures and calculated responses for Lehman Column 415. For this column, the overall simulation is very accurate, although the calculations slightly underestimate the peak strength. The hysteresis relationships for the other columns were also simulated well, but in some cases, the amount of strength degradation differed greatly between the measured and calculated responses (e.g., Fig.A.6).

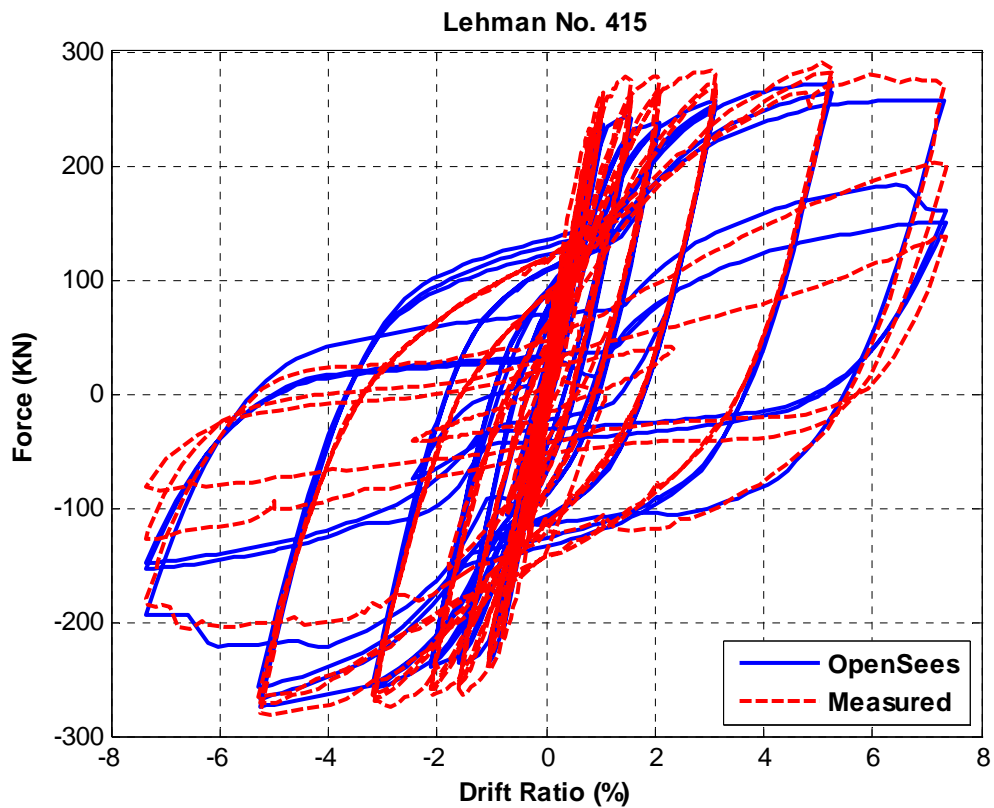


Figure 5.7. Effective force-drift response for Lehman No. 415

The measured and calculated relationships between the normalized cross-over displacement and the peak drift ratio are provided in Appendix B for all 16 tests. Figure 5.8 shows this comparison for Lehman Column 415. As shown in the figure, the analyses consistently overestimated the cross-over displacements. This trend was apparent in nearly all of the other column tests too.

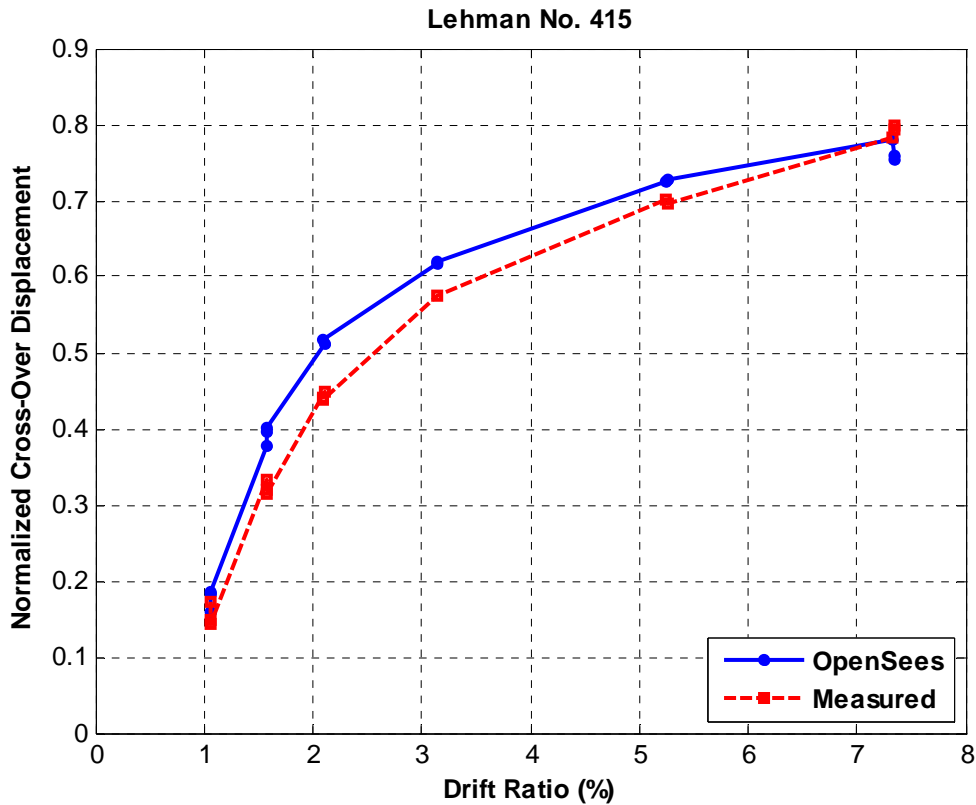


Figure 5.8. Comparison of normalized cross-over displacement vs. peak drift ratio for Lehman No. 415

5.3 PARAMETRIC STUDY WITH ANALYTICAL MODEL

A parametric study was conducted using the analytical model for the Lehman test No. 415. Four parameters for this column were varied, one at a time, to illustrate the ability of the model to capture the expected trends in cross-over displacements.

- For a given drift ratio, the cross-over displacements consistently decreased with increasing span-to-depth ratio (Fig. 5.9). This trend is consistent with the experimental data (Fig. 5.1) and Equation 5.1.
- For a given drift ratio, the cross-over displacements were consistently independent of the longitudinal reinforcement ratio. This trend is inconsistent with the experimental data. (Fig. 5.2) and Equation 5.2.
- For a given drift ratio, the cross-over displacements consistently decreased with increasing axial-load ratio (Fig. 5.11). This trend is consistent with the experimental data. (Fig. 5.3 and 5.4) and Equation 5.2.
- For a given drift ratio, the cross-over displacements consistently decreased with increasing re-centering ratio (Fig. 5.12). This trend is consistent with the experimental data. (Fig. 5.6) and Equation 5.2.

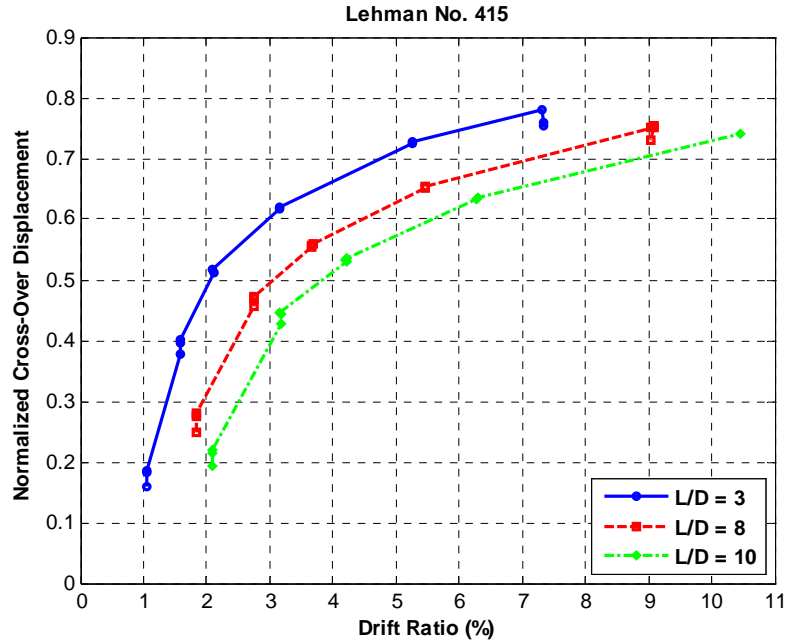


Figure 5.9. Comparison of calculated normalized cross-over displacement vs. peak drift ratio for various L/D ratios

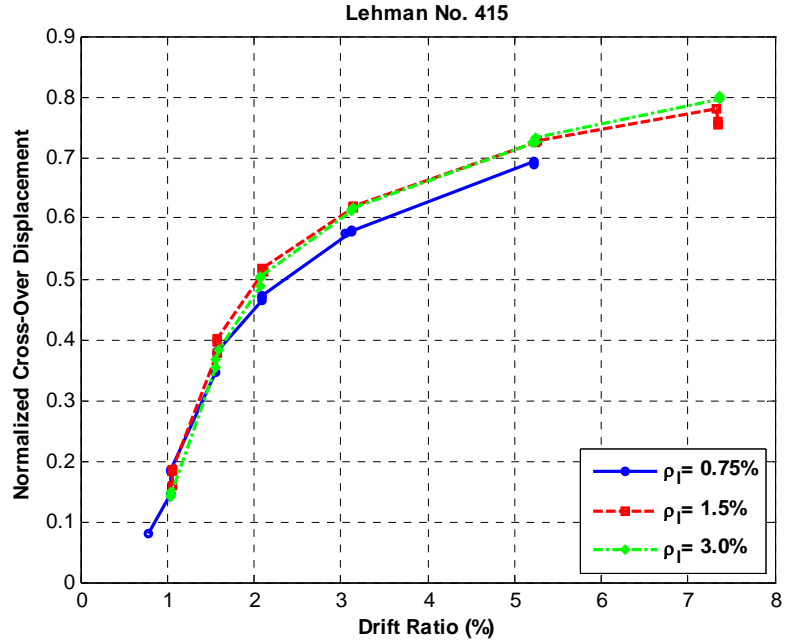


Figure 5.10. Comparison of calculated normalized cross-over displacement vs. peak drift ratio for various rho values

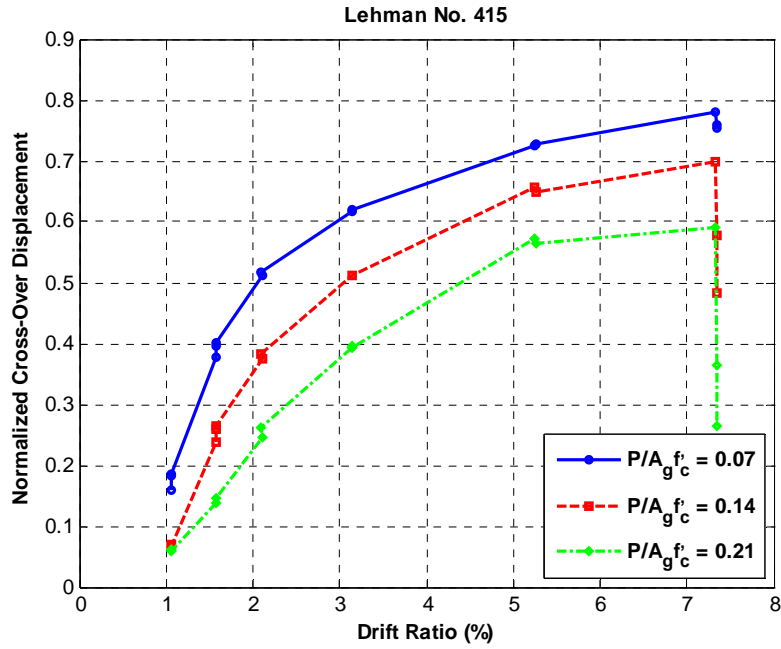


Figure 5.11. Comparison of calculated normalized cross-over displacement vs. peak drift ratio for various $P/A_g f'_c$ values

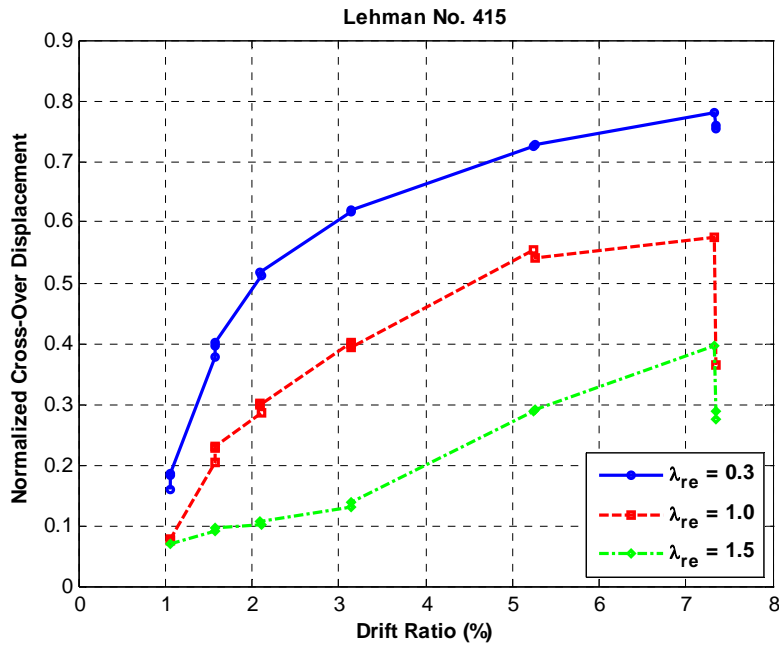


Figure 5.12. Comparison of calculated normalized cross-over displacement vs. peak drift ratio for various re-centering ratios, λ_{re}

CHAPTER 6: SUMMARY, CONCLUSIONS AND RECOMMENDATIONS

6.1 SUMMARY

The magnitude of the “residual” displacements at the end of an earthquake can affect the amount of time needed to restore a bridge to service. It may be possible to reduce these displacements by introducing prestressing forces (post-tensioning or pre-tensioning) into bridge columns. However, to design such systems, engineers need to be able to estimate the residual displacements using analytical models. This project will help establish the accuracy of the Berry and Eberhard (2007) modeling strategy.

The test data and analytical results were compared in terms of the normalized cross-over displacement, in which the cross-over displacement for each cycle was normalized by the peak displacement for that cycle.

6.2 CONCLUSIONS

Based on trends observed in sixteen tests of reinforced concrete column, the normalized cross-over displacement decreases with:

- decreases in peak drift ratio
- increases in span-to-depth ratio
- decreases in reinforcement ratio
- increases in axial-load ratio, and
- increases in the re-centering ratio.

The model did reproduce the expected trends in peak drift ratio, span-to-depth ratio, axial load ratio and re-centering ratio, but it did not reproduce the observed trend in longitudinal reinforcement ratio. The analytical estimates of the cross-over ratios consistently exceeded the measured values by approximately 20%.

6.3 RECOMMENDATIONS

Additional research is needed to establish a statistical correlation between the cross-over displacement and the residual displacement for suites of earthquakes. Once this information is added to the results of this study, it will then be possible to develop tools to help designers evaluate the benefits of introducing prestressing into reinforced concrete bridge columns.

REFERENCES

1. Berry, M.P. and Eberhard, M.O. (2007). "Performance Modeling Strategies for Modern Reinforced Concrete Columns," Pacific Earthquake Engineering Research Center Report, PEER 2007/7, University of California, Berkeley, July, 206 pp.
2. Berry, M. P., Parrish, M. and Eberhard, M.O. (2004), "PEER Structural Performance Database User's Manual," Pacific Earthquake Engineering Research Center report, University of California, Berkeley.
3. Calderone, A.J., Lehman, D.E., Moehle, J.P. (2000), "Behavior of Reinforced Concrete Bridge Columns Having Varying Aspect Ratios and Varying Lengths of Confinement," Pacific Earthquake Engineering Research Center Report 2000/08.
4. Cheok, G.S. and Stone, William C. (1986), Behavior of 1/6-Scale Model Bridge Columns Subjected to Cycle Inelastic Loading, NBSIR 86-3494, Center for Building Technology, National Engineering Laboratory, National Institute of Standards and Technology, Gaithersburg, Maryland, 20899, November, 291 pages.
5. Cohagen, L.S. Pang, J.B.K., Steuck, K.P., Eberhard, M.O. and Stanton, J.F. (2008), "A Precast Concrete Bridge Bent Designed to Re-center after an Earthquake," Washington State Department of Transportation Report, WA-RD 684.3, Olympia, Washington, October, 184 pp.
6. Hieber, D.G., Wacker, J.M., Eberhard, M.O. and Stanton, J.F. (2005), "Precast Concrete Pier Systems for Rapid Construction of Bridges in Seismic Regions," Washington State Department of Transportation Report WA-RD 611.1, Olympia, Washington, March, 312 pp.
7. Kowalsky, M.J., Priestley, M.J.N., and Seible, F (1999), "Shear and Flexural Behavior of Lightweight Concrete Bridge Columns in Seismic Regions," American Concrete Institute, ACI Structural Journal, Vol. 96, No. 1, January-February, pp. 136-148.

8. Lehman, D.E. and Moehle, J.P. (2000); "Seismic Performance of Well-Confined Concrete Bridge Columns," Pacific Earthquake Engineering Research Center, PEER 1998/01, Dec.
9. OpenSees Development Team (2010). Opensees: Open system for earthquake engineering simulations. Version 2.21, Berkeley, CA.
10. Pang, J.B.K., Stanton, J.F., Eberhard, M.O. (2008a), "Precast Bridge Bent Connection for Rapid Construction in Seismic Regions." Proceedings, 2008 FHWA Accelerated Bridge Construction Conference, Baltimore, Maryland, March 20-21.
11. Pang, J.B.K., Stanton, J.F., Eberhard, M.O. (2008b), "Large-Bar Connection for Precast Bridge Bents in Seismic Regions." Proceedings, IABSE Annual Meeting and Congress, Chicago, Illinois, September 14-19.
12. Pang, J.B.K., Steuck, K.P., Cohagen, L.S., Eberhard, M.O. and Stanton, J.F. (2008c), "Rapidly Constructible Large-Bar Precast Bridge-Bent Connection," Washington State Department of Transportation Draft Report, WA-RD 684.2, Olympia, Washington, October, 184 pp.
13. Pang, B.K., Eberhard, M.O., and Stanton, J.F. (2010), "Large-Bar Connection for Precast Bridge Bents in Seismic Regions," Journal of Bridge Engineering, ASCE, May-June, pp 231-239.
14. Scott, M. and G. Fenves (2006). Plastic hinge integration methods for force-based beam-column elements. Journal of the Structural Engineering ASCE 132(2), 244–252.
15. Steuck, K., Stanton, J.F. and Eberhard, M.O. (2009), "Anchorage of Large-Diameter Reinforcing Bars in Ducts," ACI Structural Journal, July-August, pp 506-513.

APPENDIX A:

**MEASURED AND CALCULATED
EFFECTIVE FORCE - DRIFT RATIO
HYSTERETIC RELATIONSHIPS**

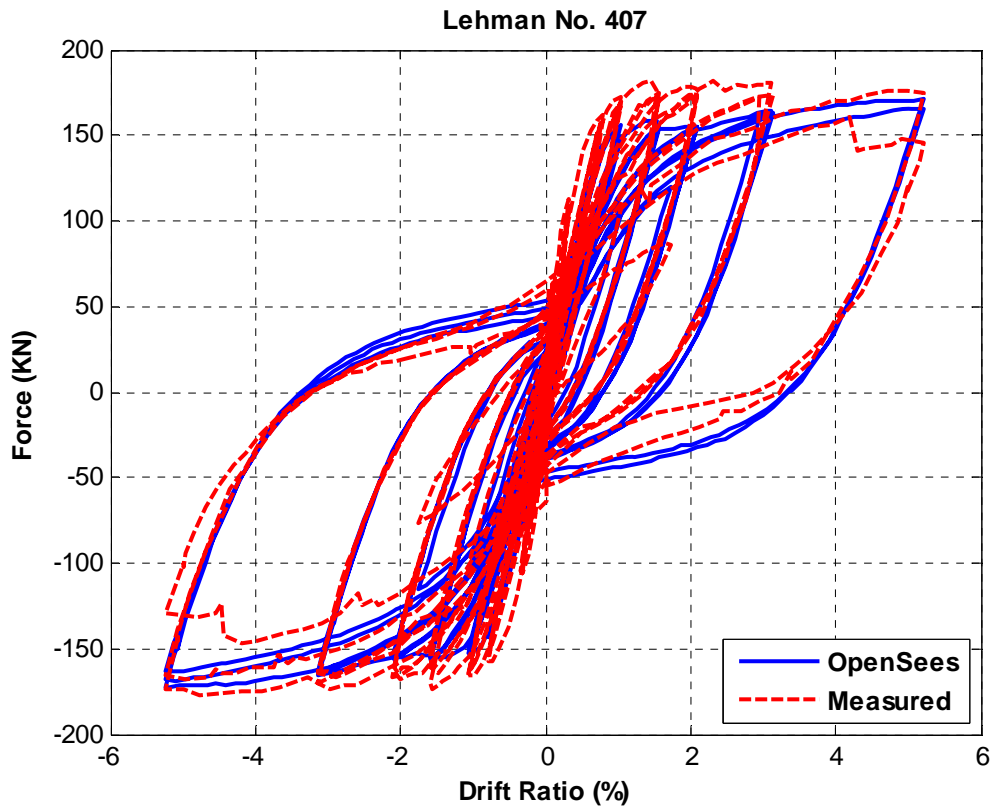


Figure A.1. Effective force-drift response for Lehman No. 407

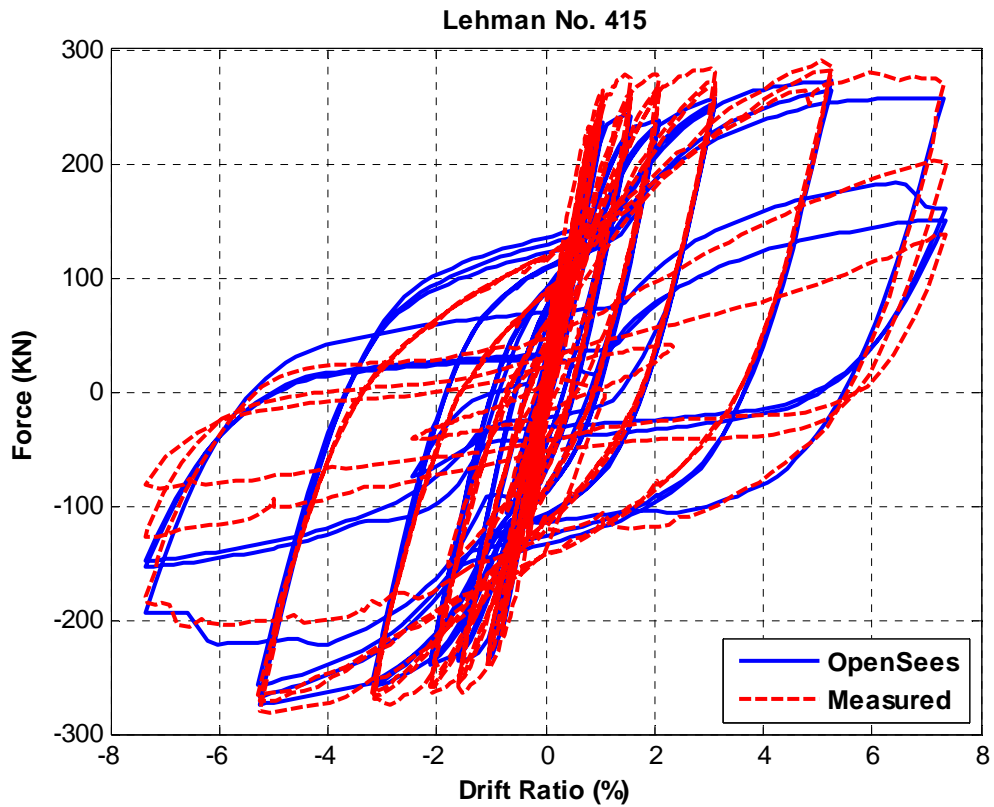


Figure A.2. Effective force-drift response for Lehman No. N415

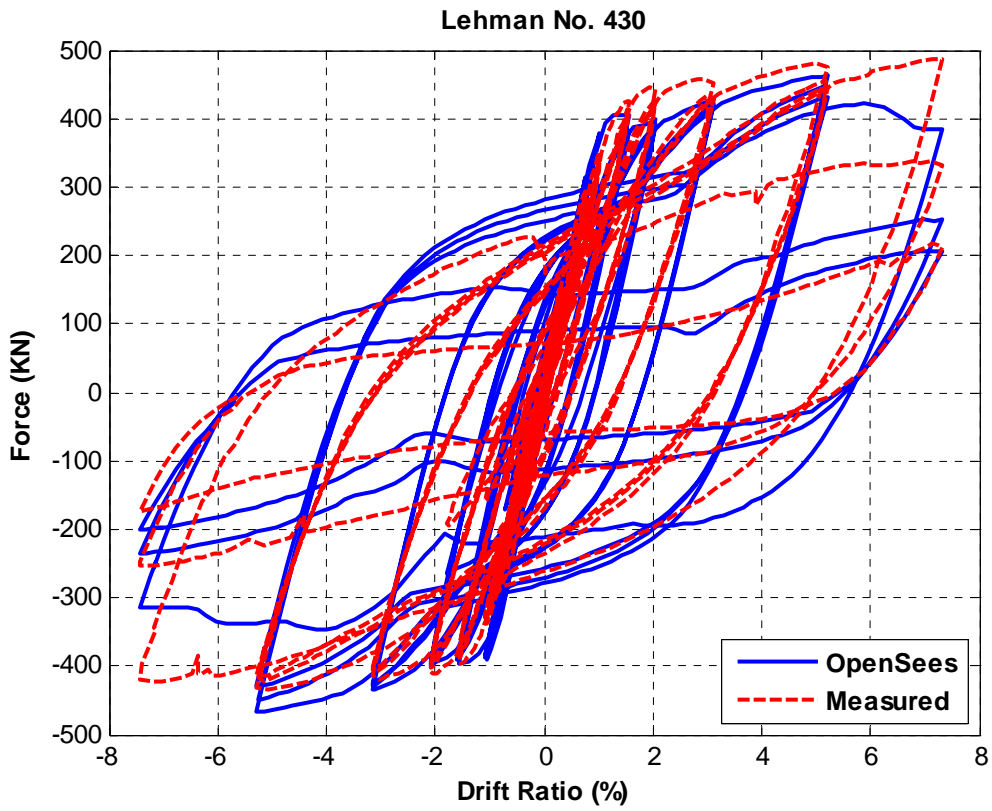


Figure A.3. Effective force-drift response for Lehman No. 430

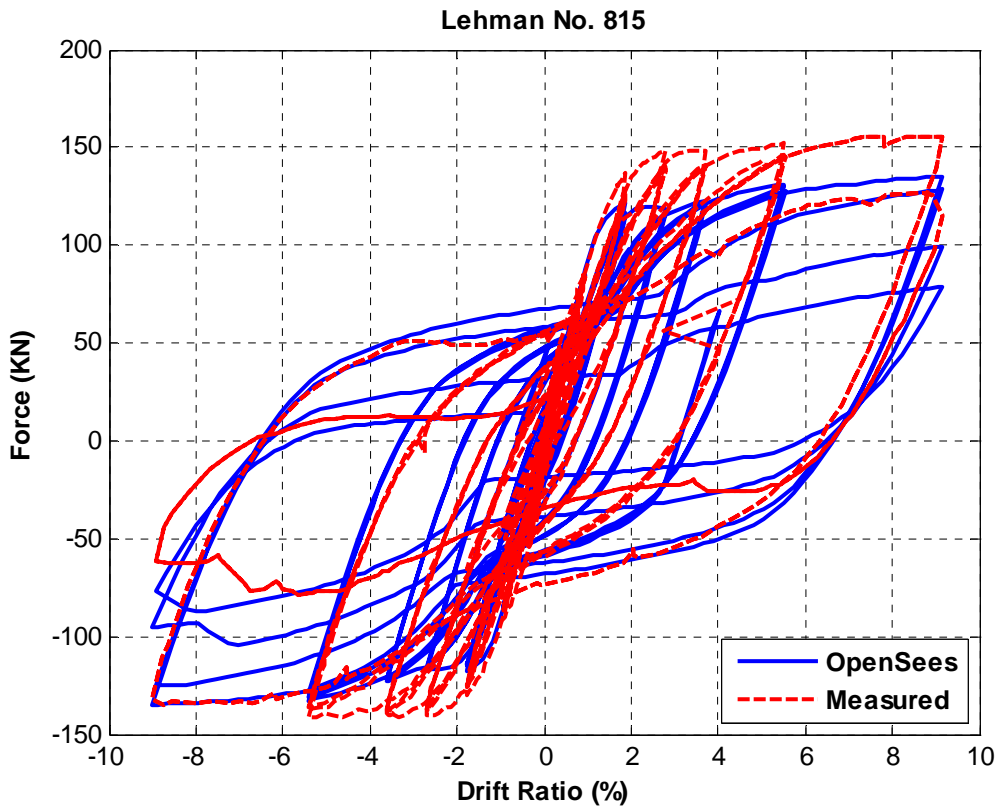


Figure A.4. Effective force-drift response for Lehman No. 815

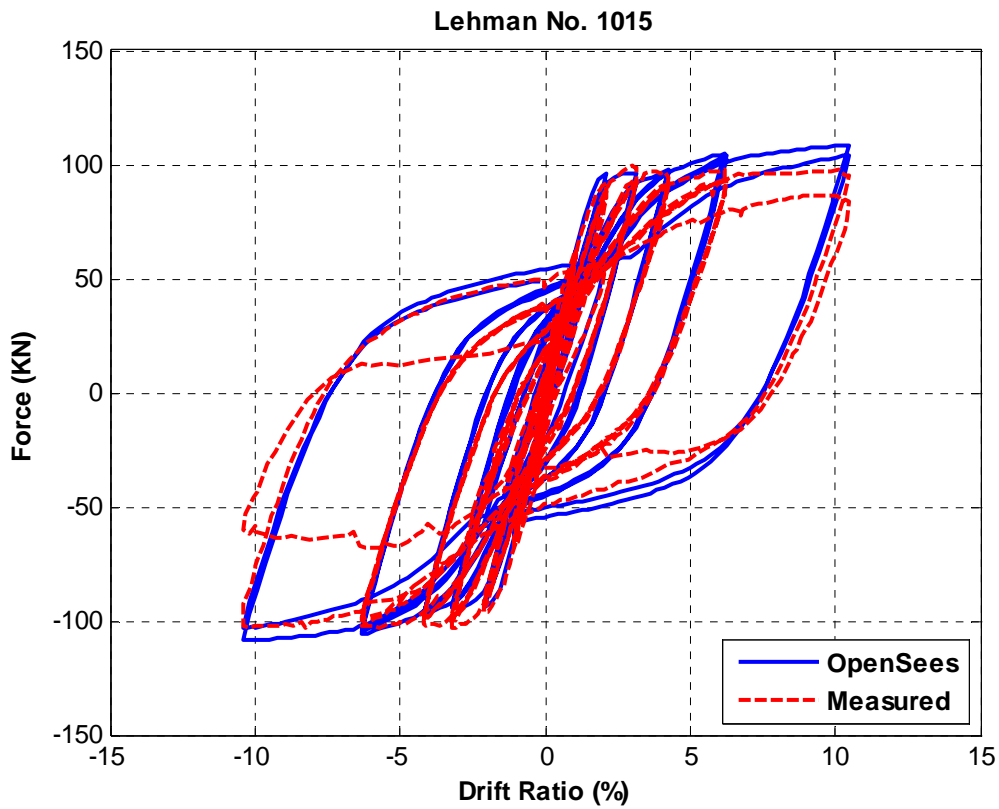


Figure A.5. Effective force-drift response for Lehman No. 1015

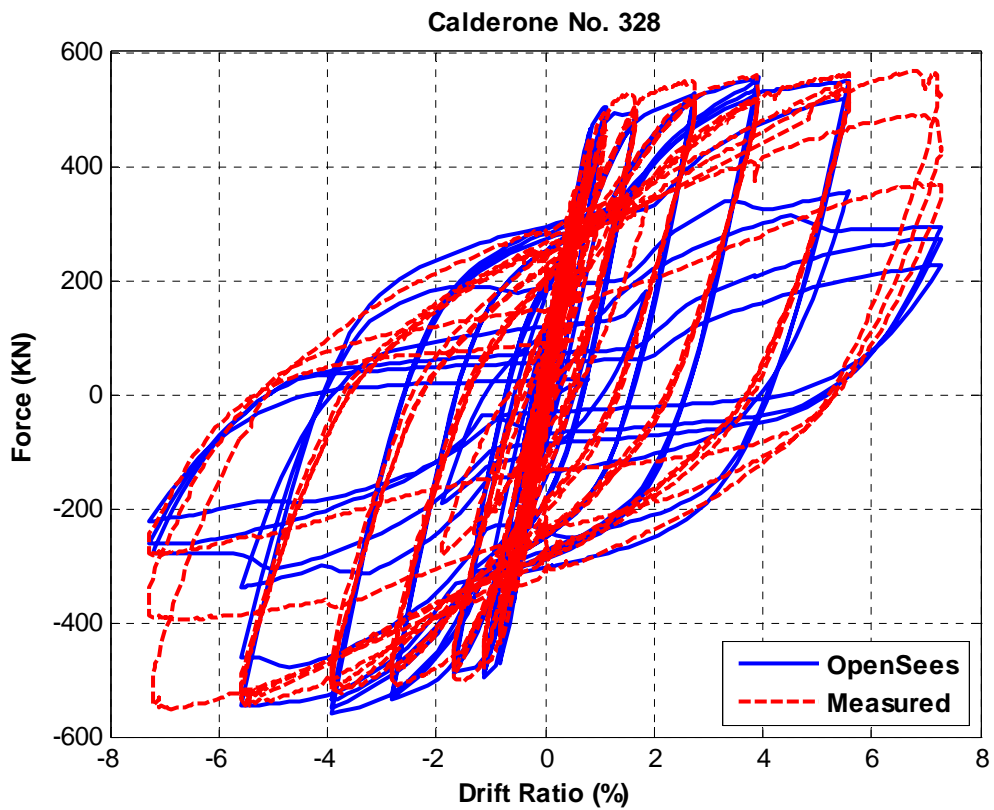


Figure A.6. Effective force-drift response for Calderone No. 328

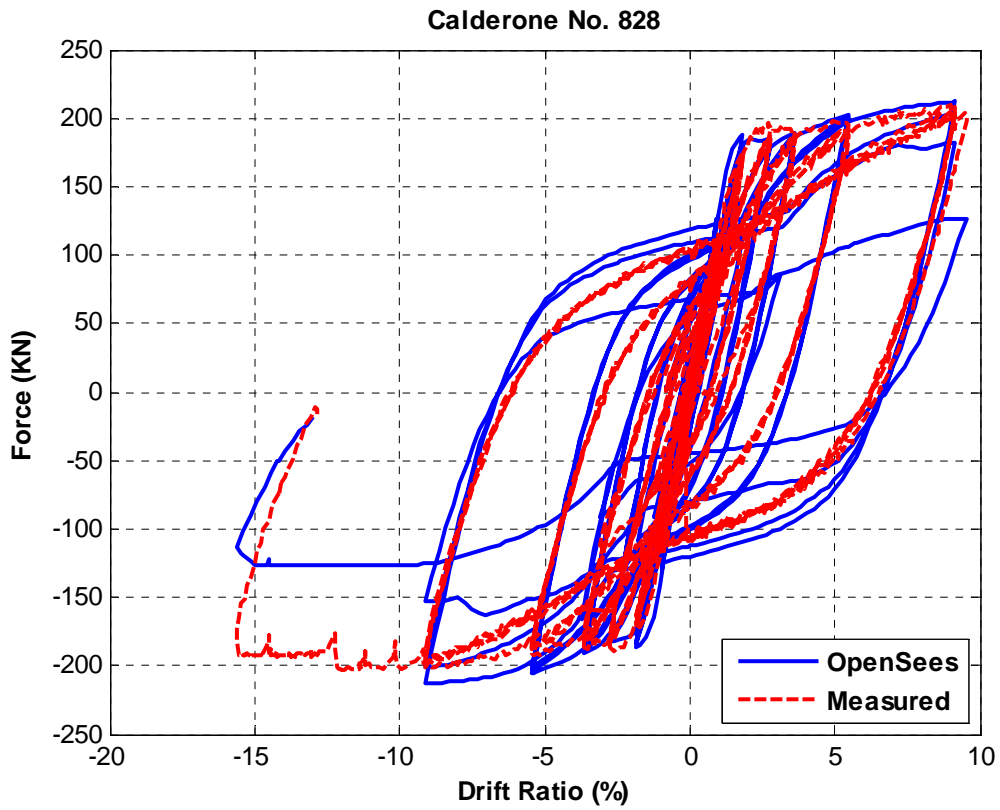


Figure A.7. Effective force-drift response for Calderone No. 828

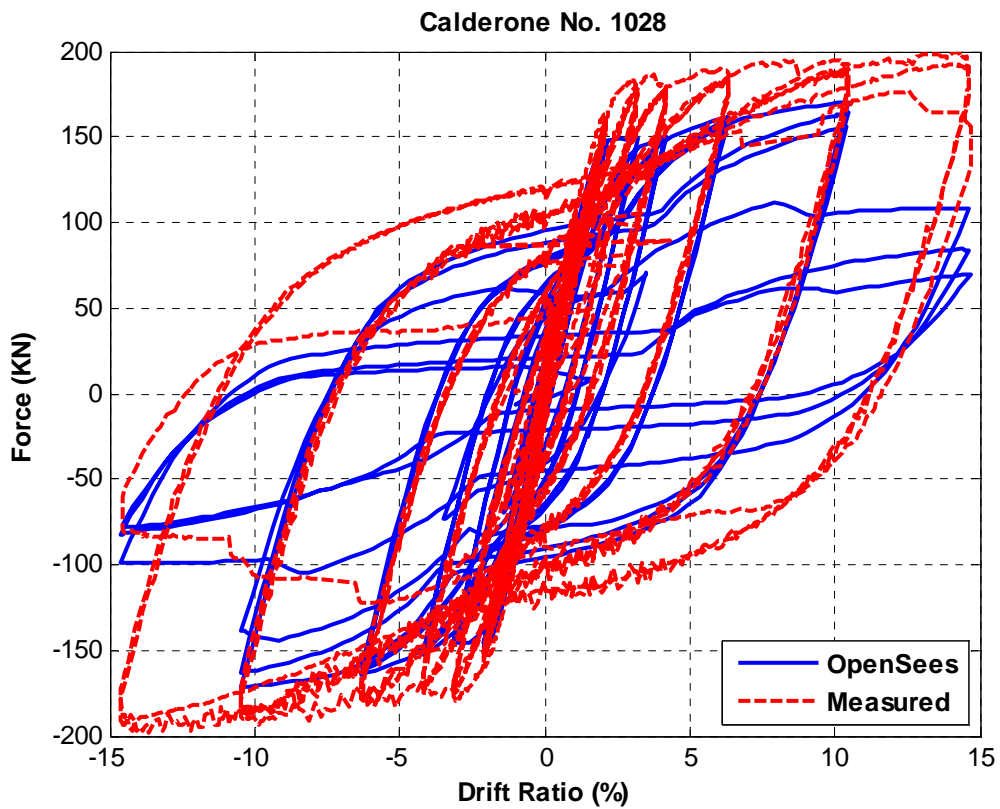


Figure A.8. Effective force-drift response for Calderone No. 1028

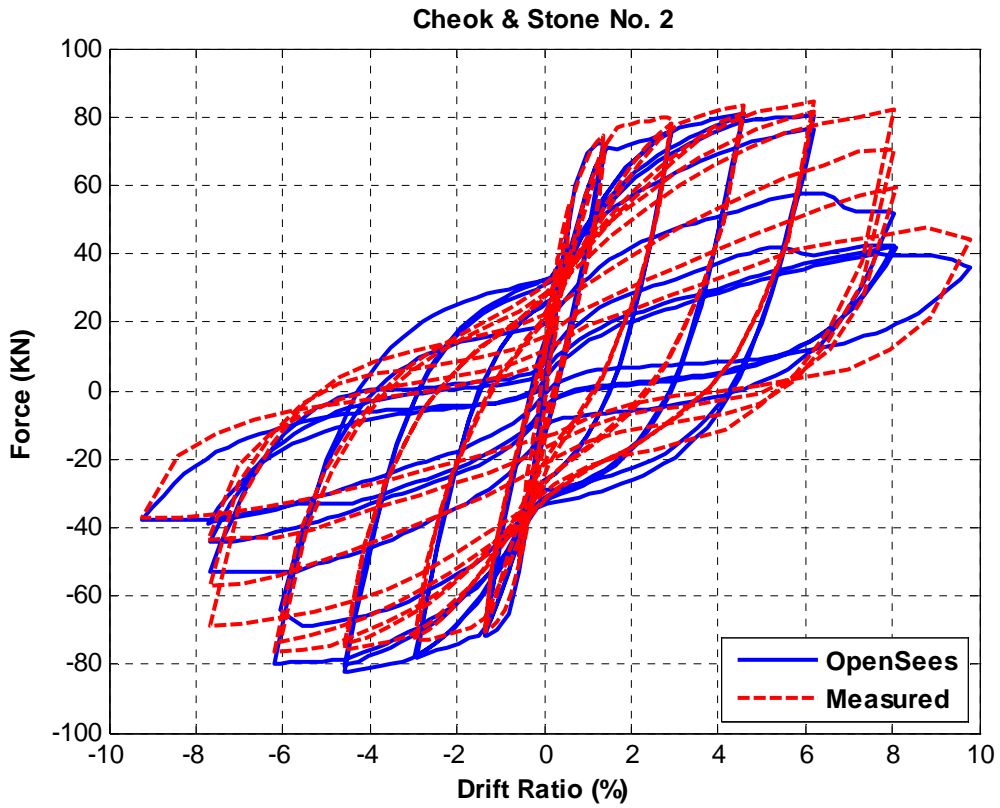


Figure A.9. Effective force-drift response for Cheek & Stone No. 2

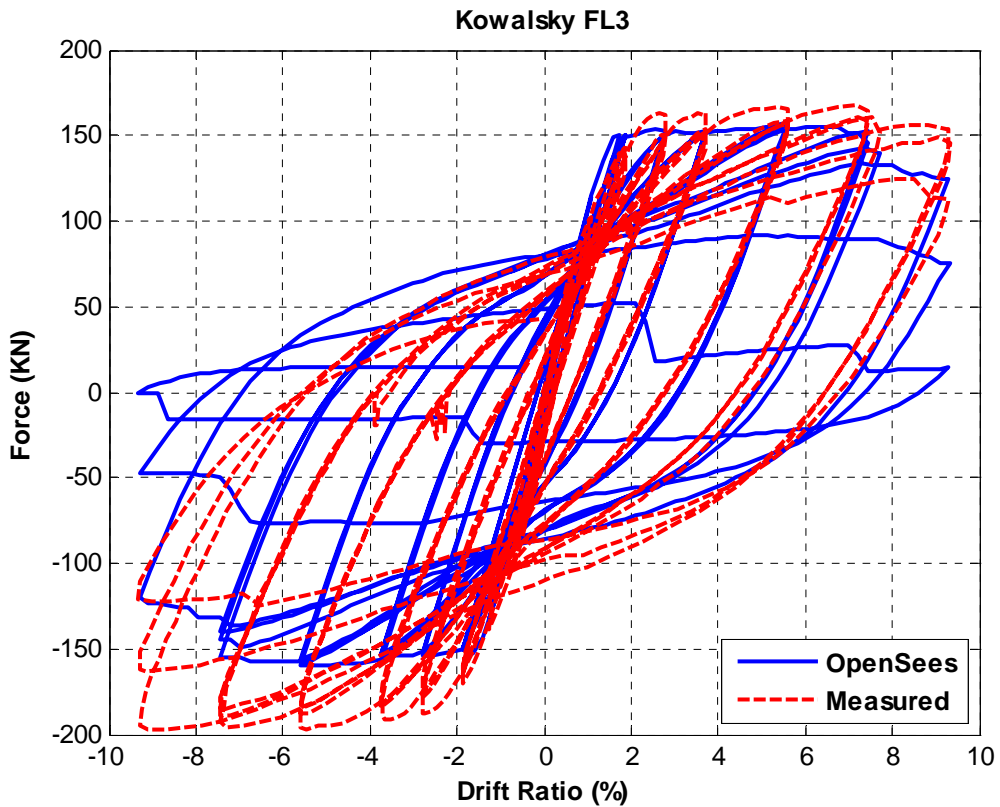


Figure A.10. Effective force-drift response for Kowalsky FL3

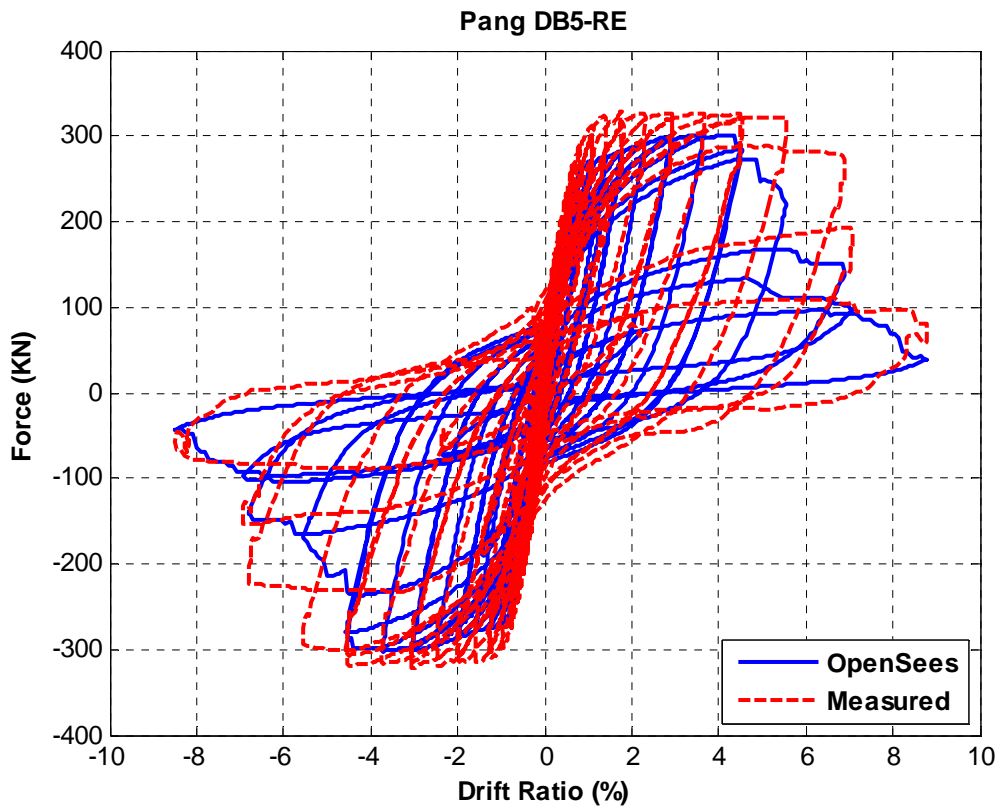


Figure A.11. Effective force-drift response for Pang LB8-RE

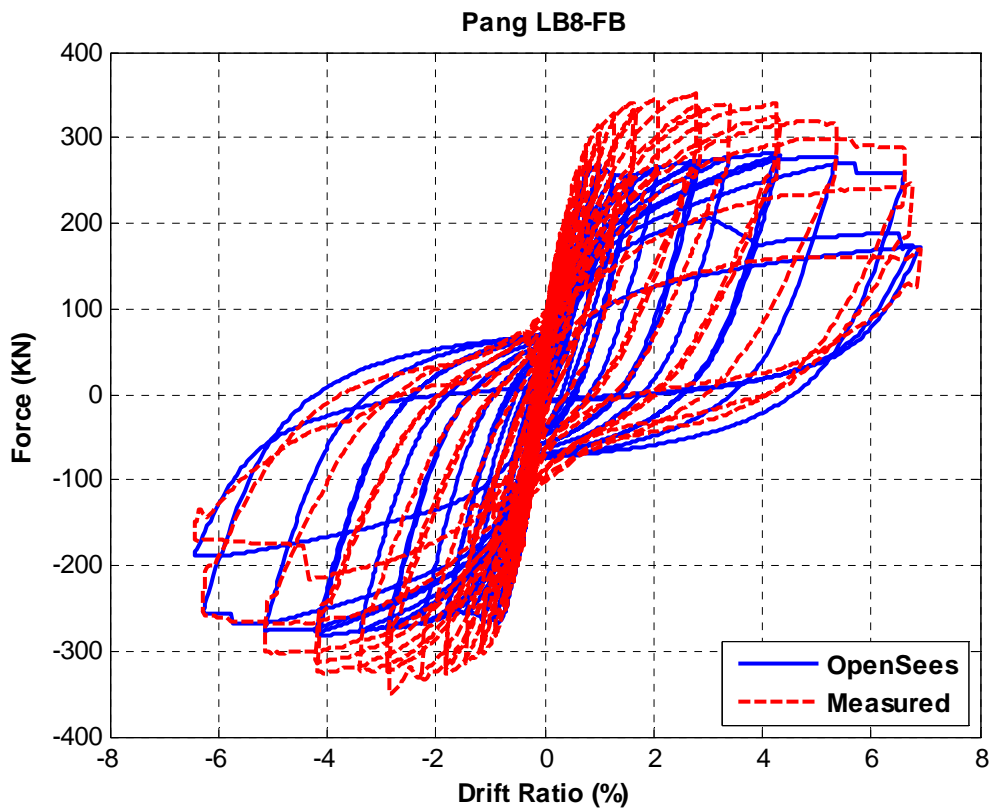


Figure A.12. Effective force-drift response for Pang LB8-FB

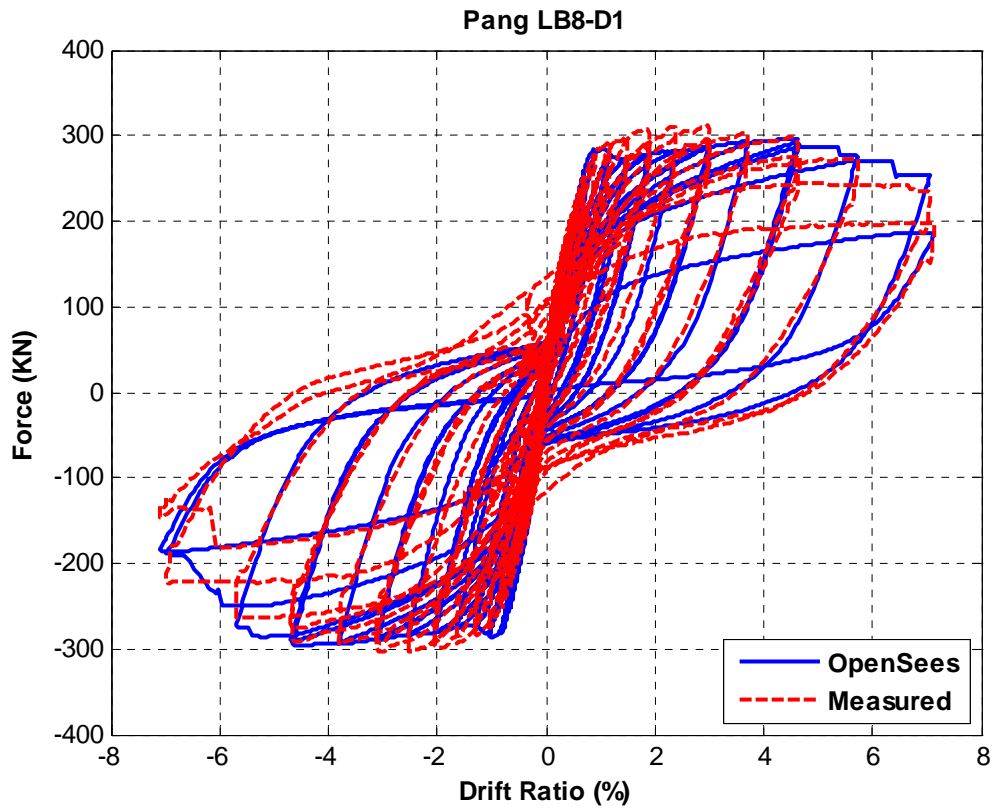


Figure A.13. Effective force-drift response for Pang LB8-D1

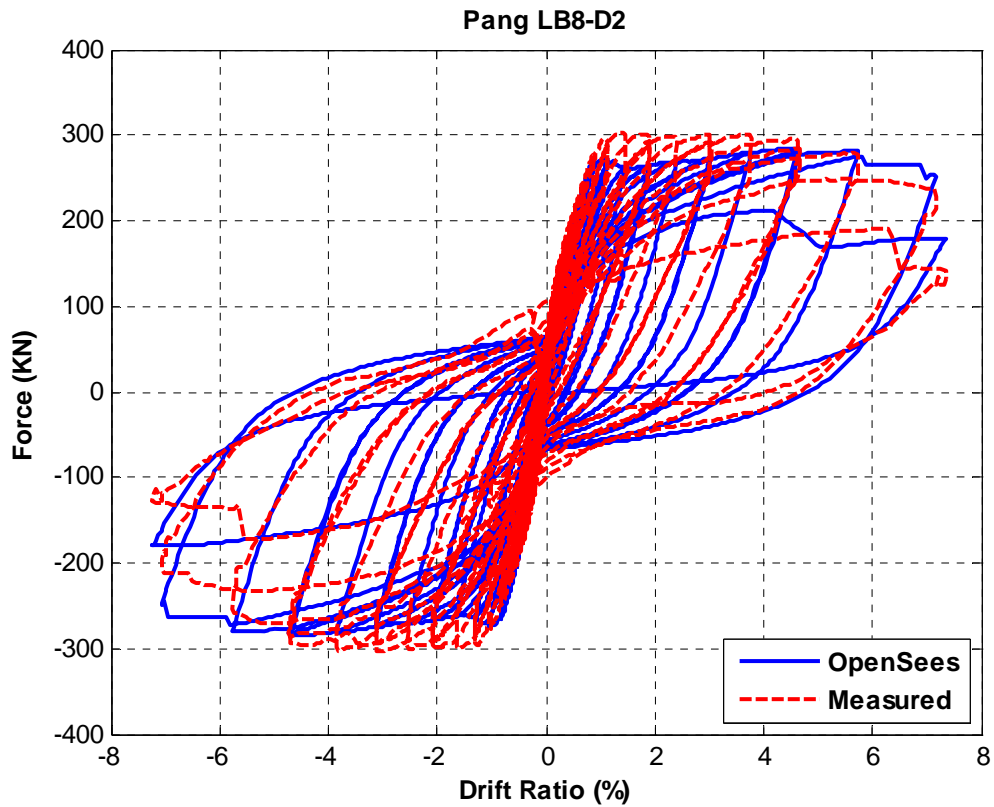


Figure A.14. Effective force-drift response for Pang LB8-D2

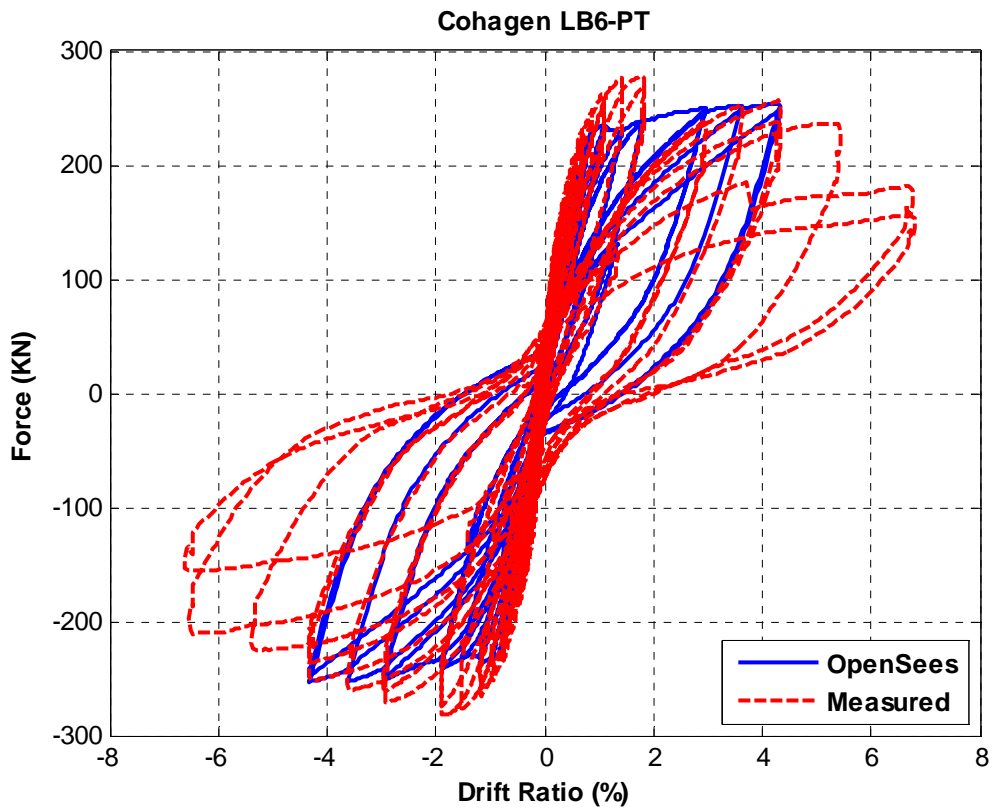


Figure A.15. Effective force-drift response for Cohagen LB6-PT

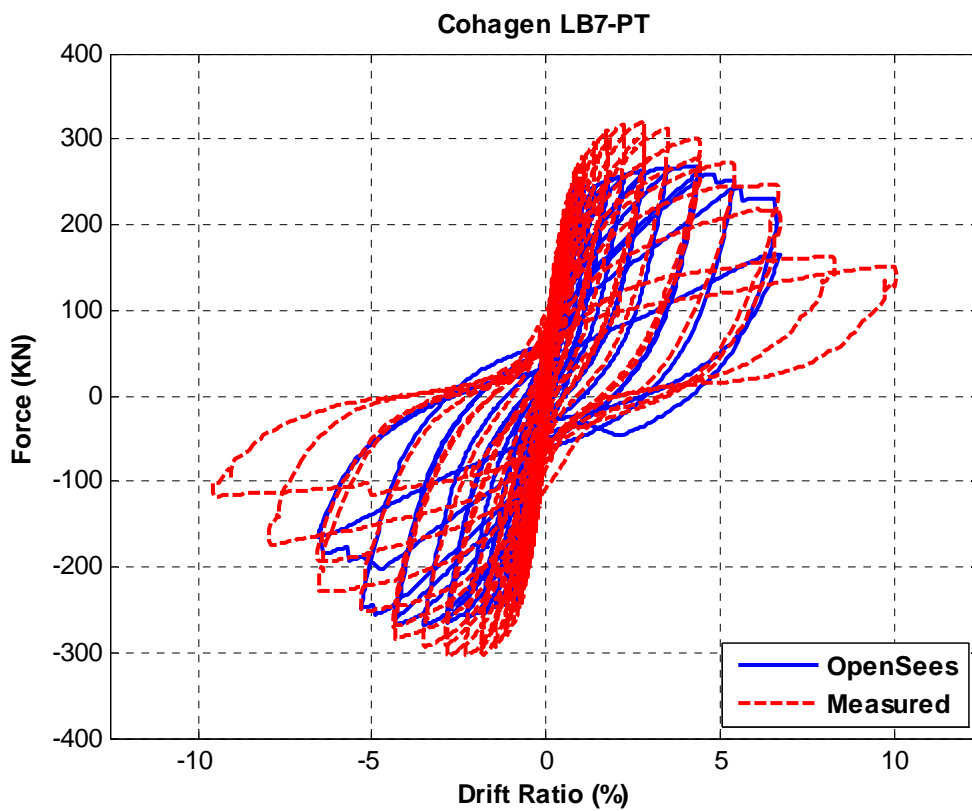


Figure A.16. Effective force-drift response for Cohagen LB7-PT

APPENDIX B:

**MEASURED AND CALCULATED
NORMALIZED CROSS-OVER DISPLACEMENT VERSUS
PEAK DRIFT RATIO**

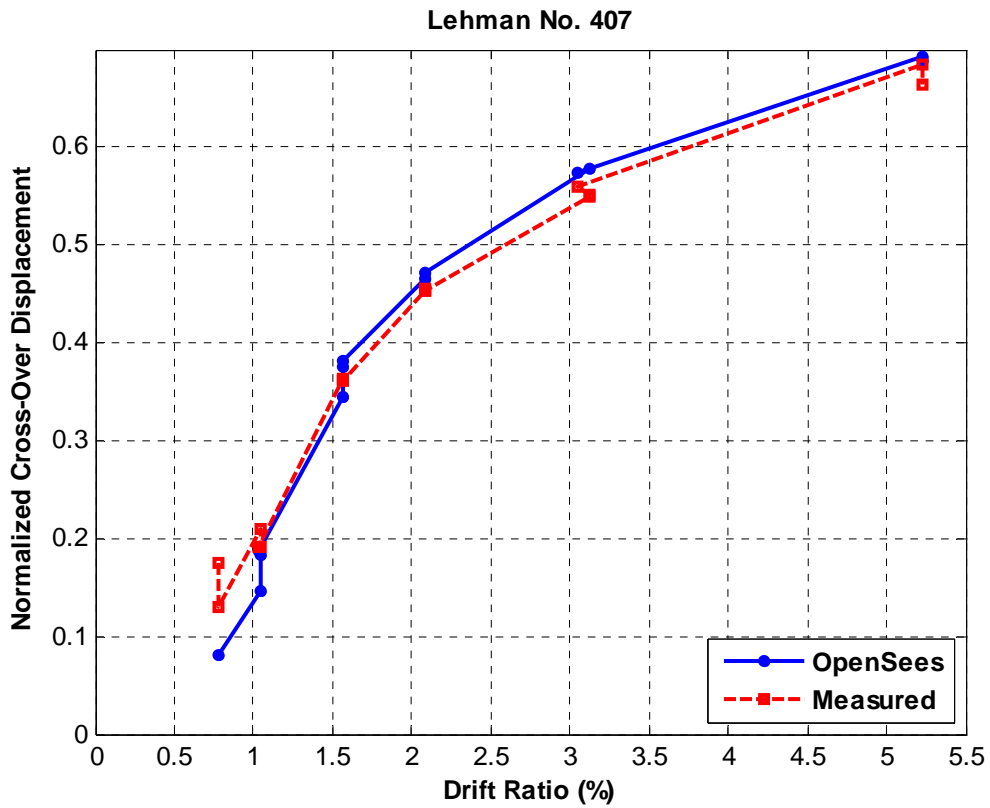


Figure B.1. Comparison of normalized cross-over displacement vs. peak drift ratio for Lehman No. 407

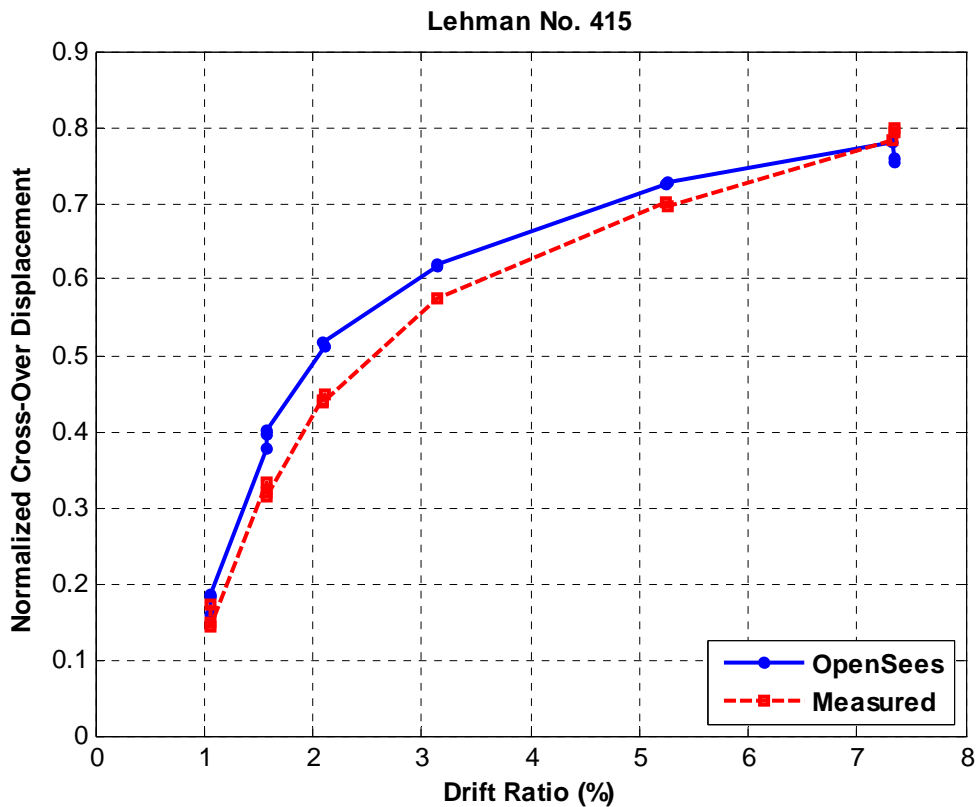


Figure B.2. Comparison of normalized cross-over displacement vs. peak drift ratio for Lehman No. 415

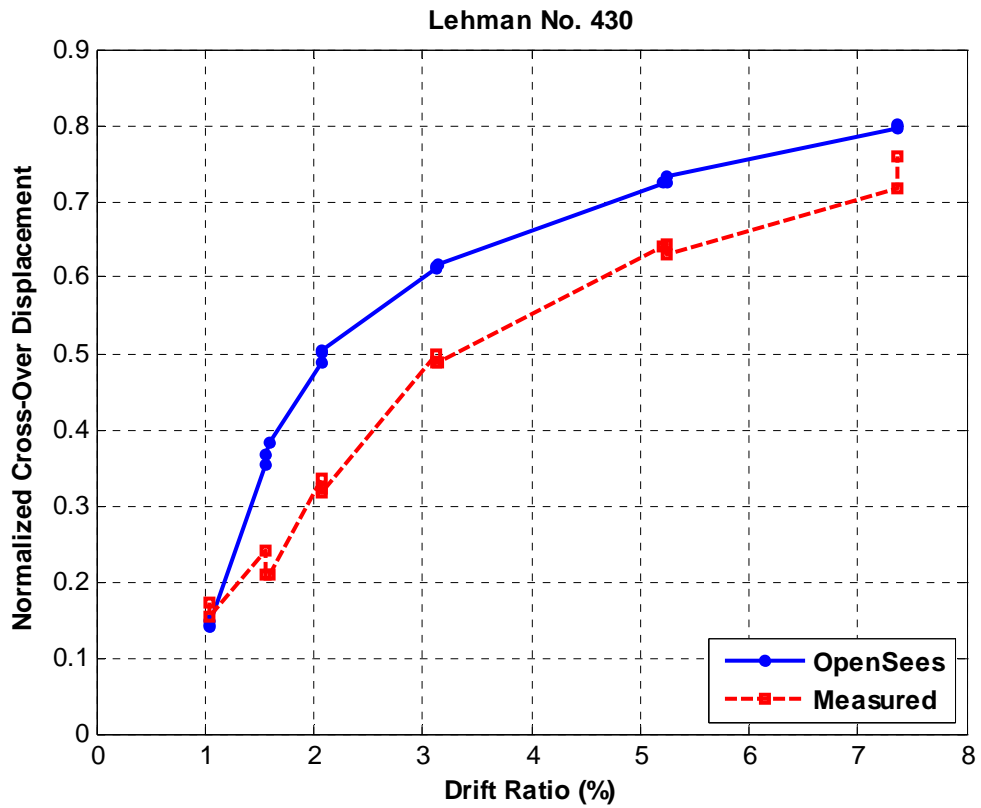


Figure B.3. Comparison of normalized cross-over displacement vs. peak drift ratio for Lehman No. 430

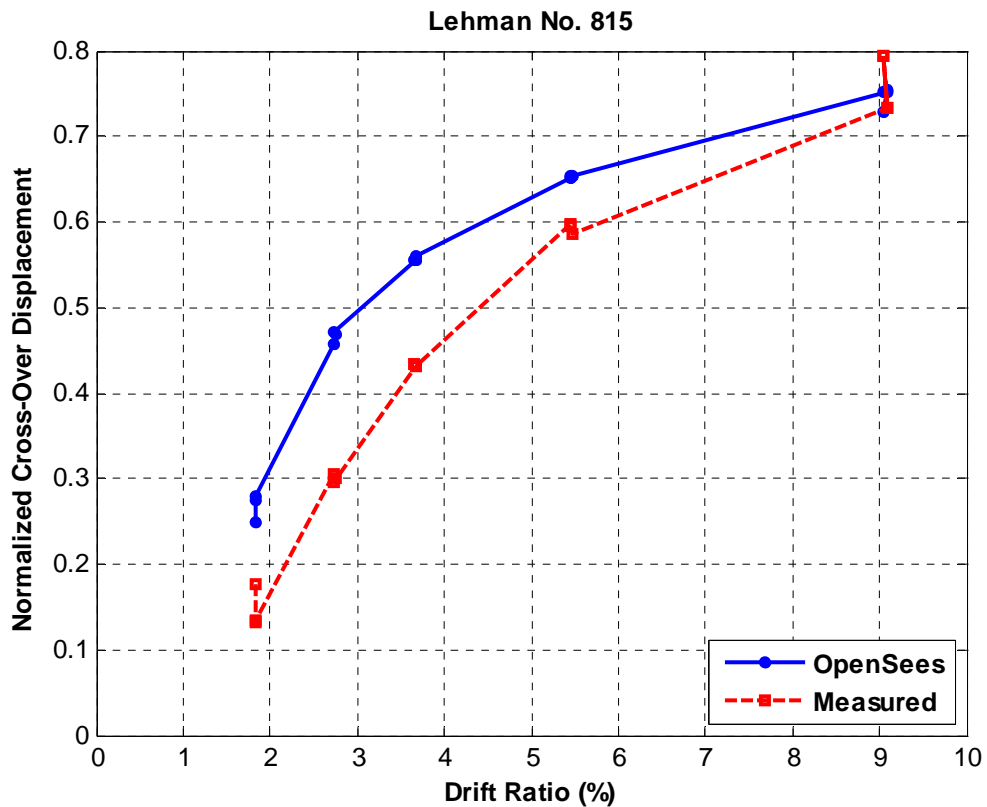


Figure B.4. Comparison of normalized cross-over displacement vs. peak drift ratio for Lehman No. 815

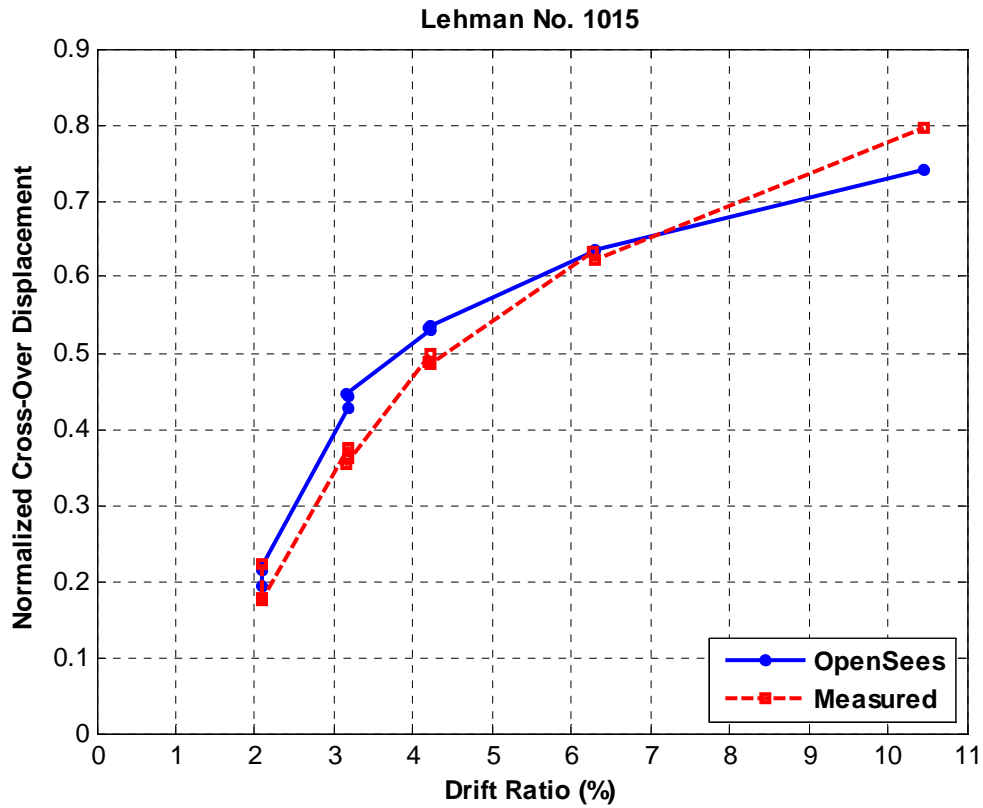


Figure B.5. Comparison of normalized cross-over displacement vs. peak drift ratio for Lehman No. 1015

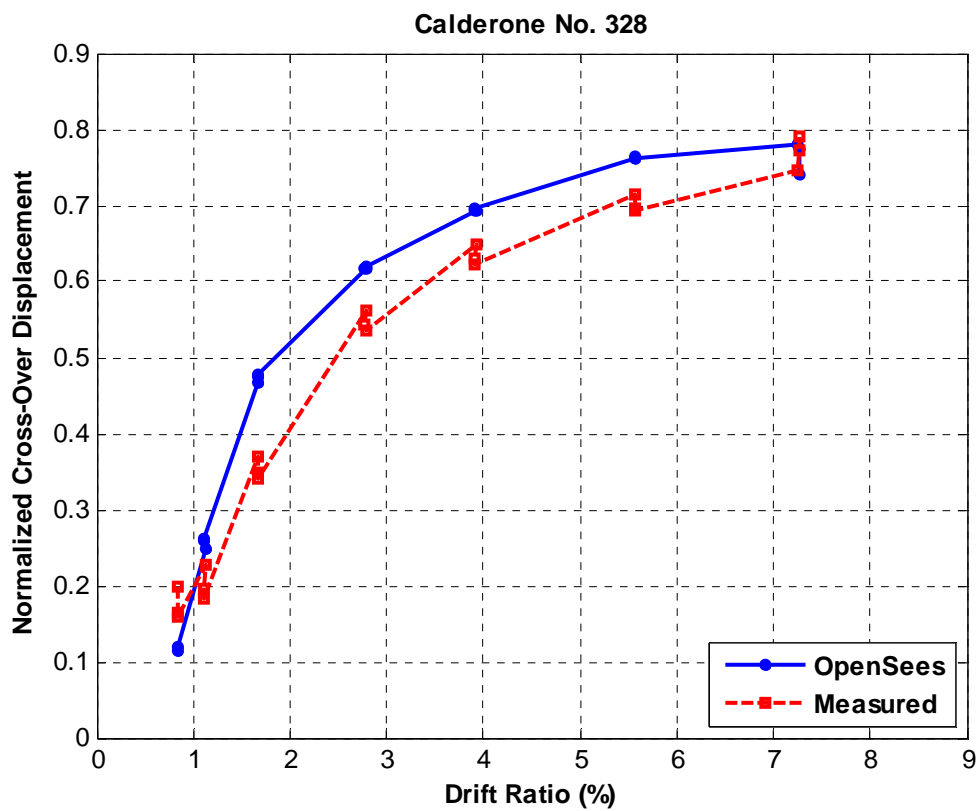


Figure B.6. Comparison of normalized cross-over displacement vs. peak drift ratio for Calderone No. 328

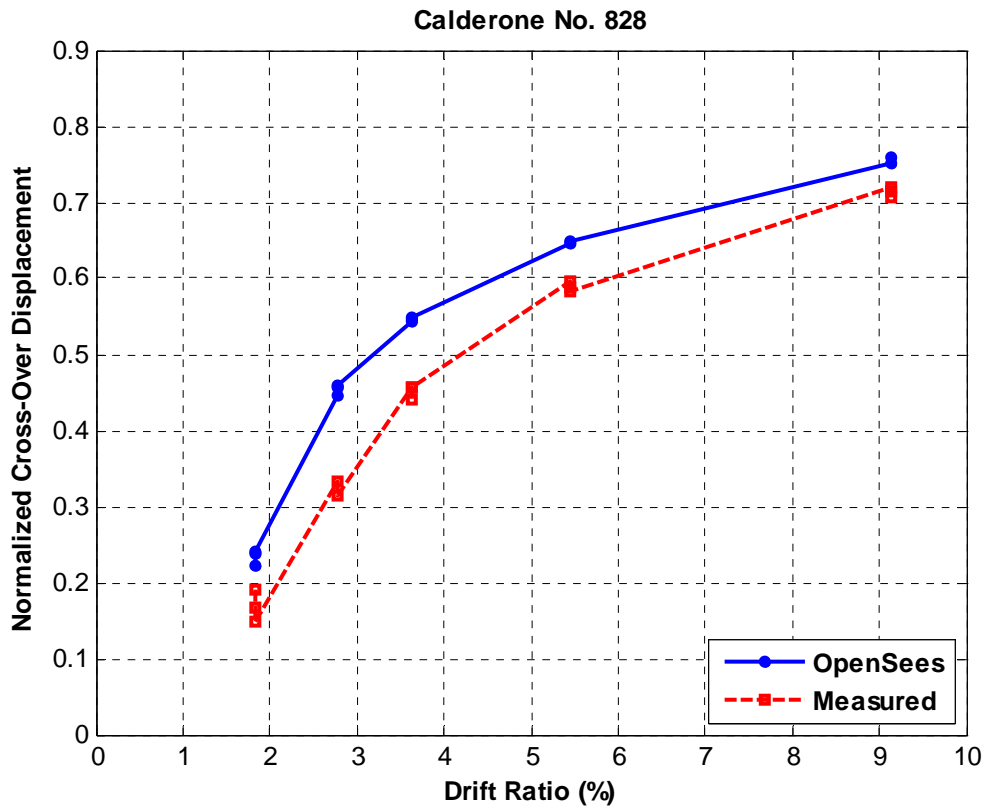


Figure B.7. Comparison of normalized cross-over displacement vs. peak drift ratio for Calderone No. 828

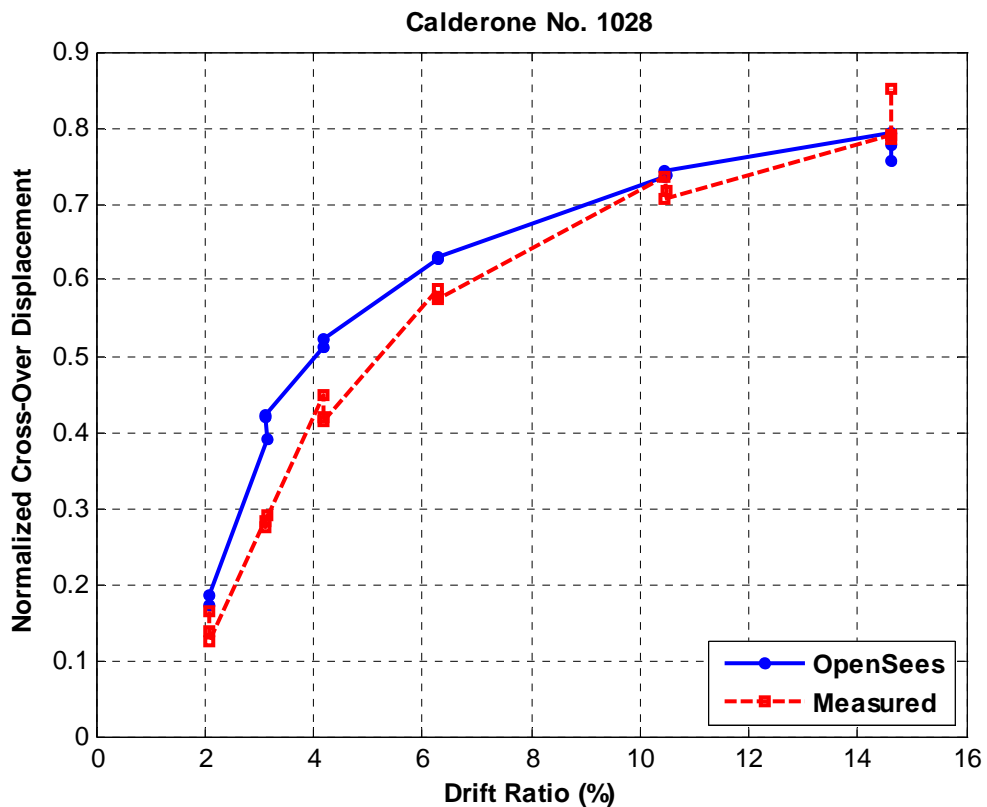


Figure B.8. Comparison of normalized cross-over displacement vs. peak drift ratio for Calderone No. 1028

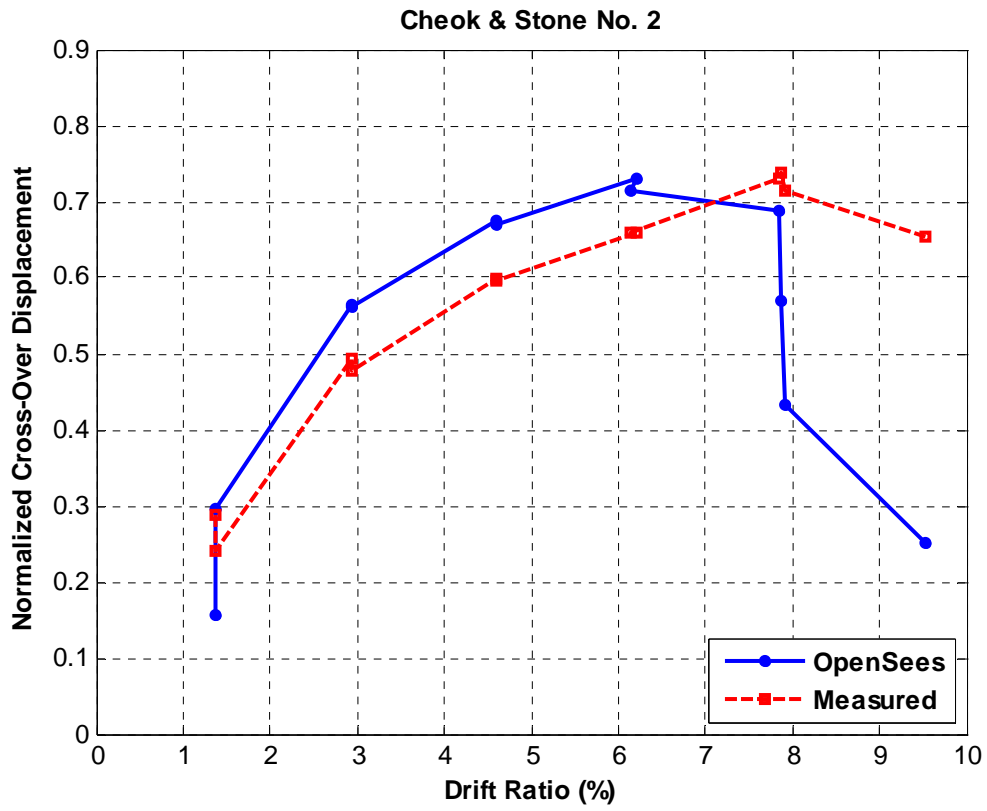


Figure B.9. Comparison of normalized cross-over displacement vs. peak drift ratio for Cheek & Stone No. 2

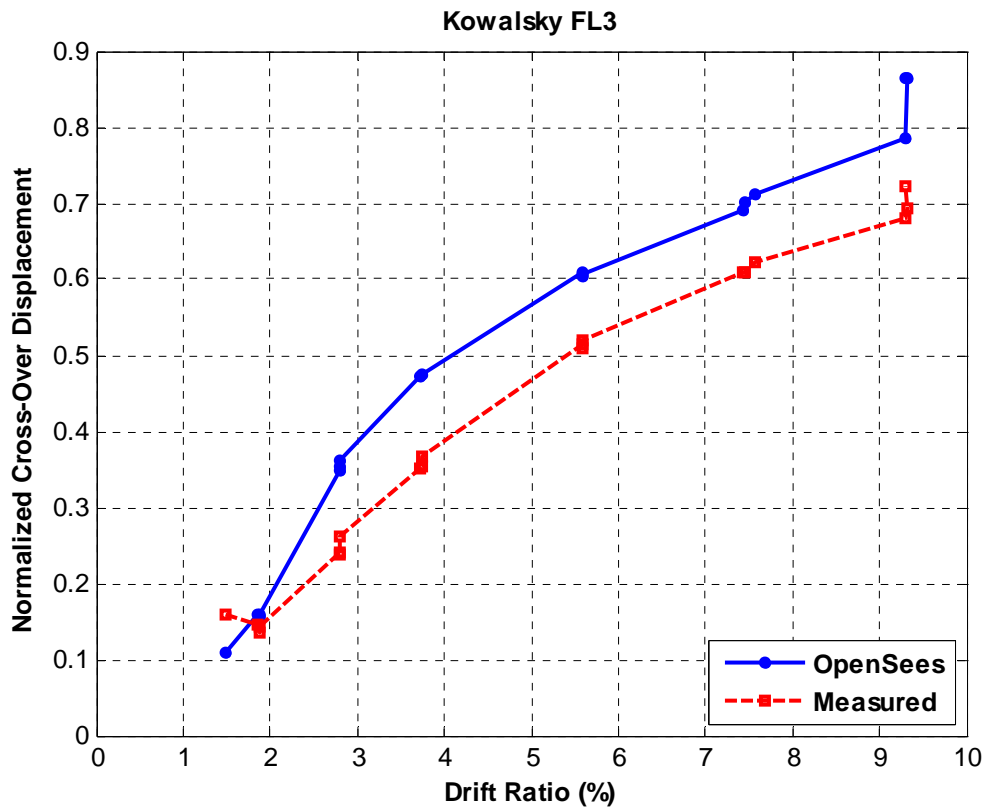


Figure B.10. Comparison of normalized cross-over displacement vs. peak drift ratio for Kowalsky FL3

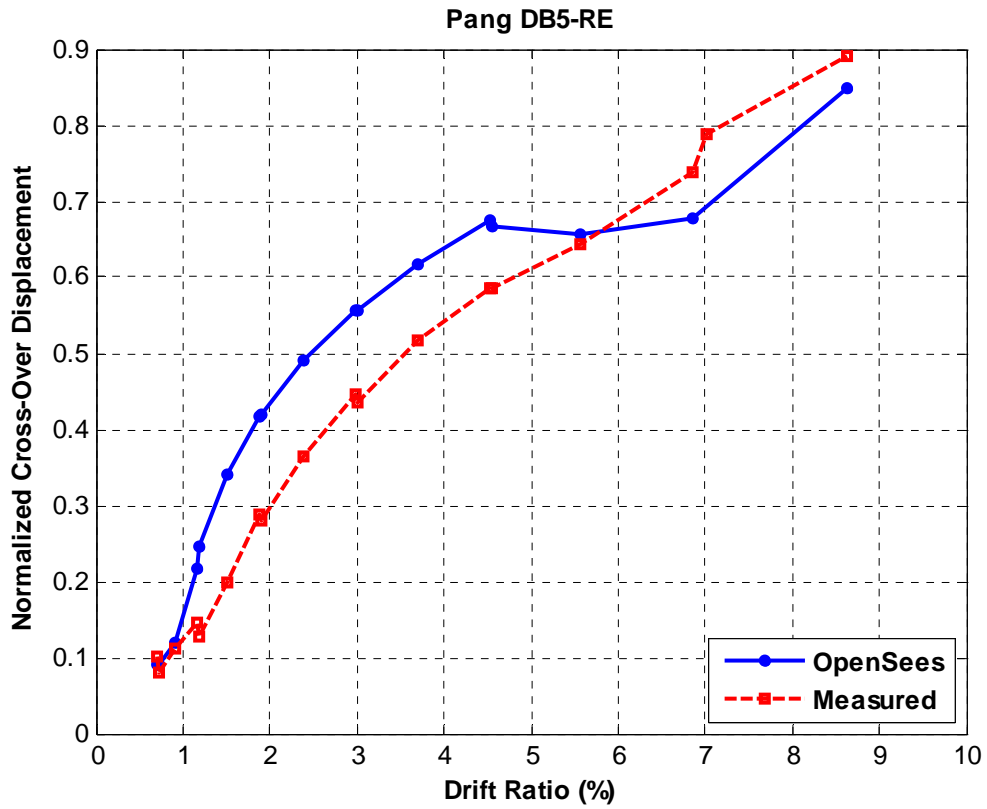


Figure B.11. Comparison of normalized cross-over displacement vs. peak drift ratio for Pang LB8-RE

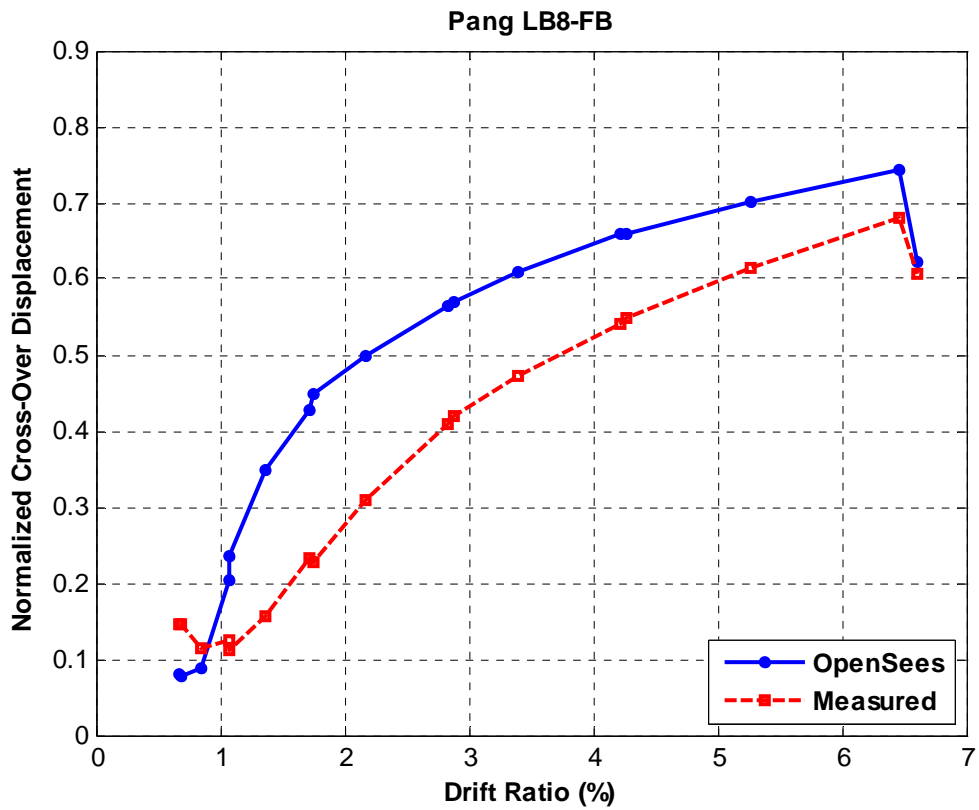


Figure B.12. Comparison of normalized cross-over displacement vs. peak drift ratio for Pang LB8-FD

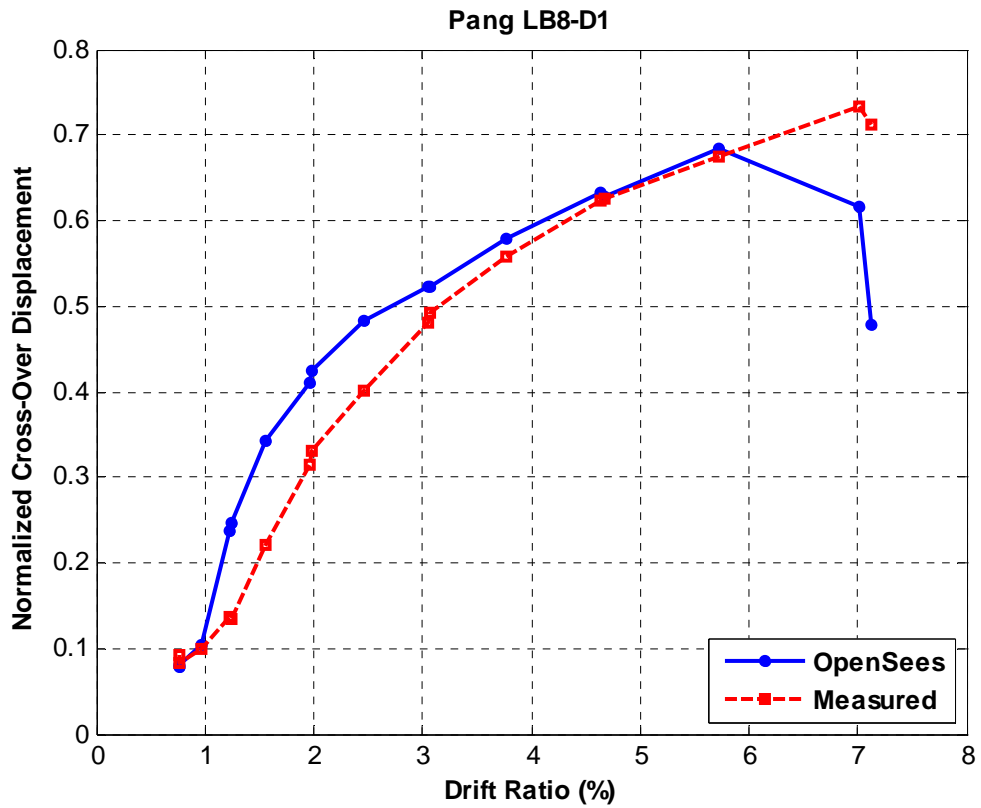


Figure B.13. Comparison of normalized cross-over displacement vs. peak drift ratio for Pang LB8-D1

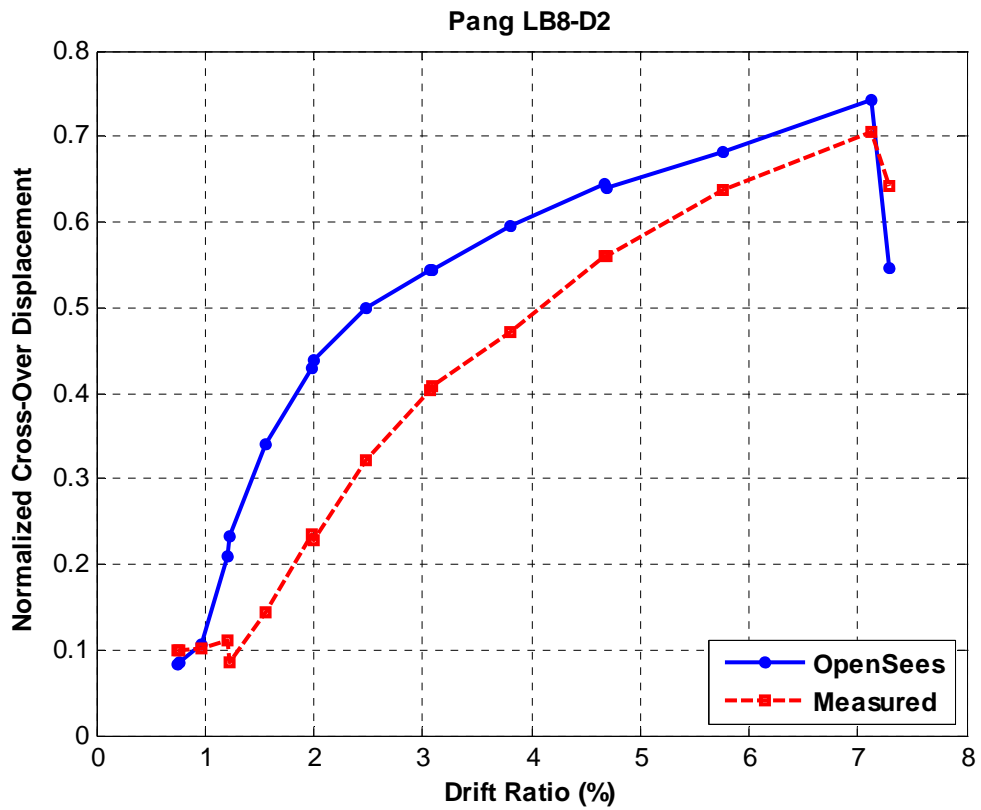


Figure B.14. Comparison of normalized cross-over displacement vs. peak drift ratio for Pang LB8-D1

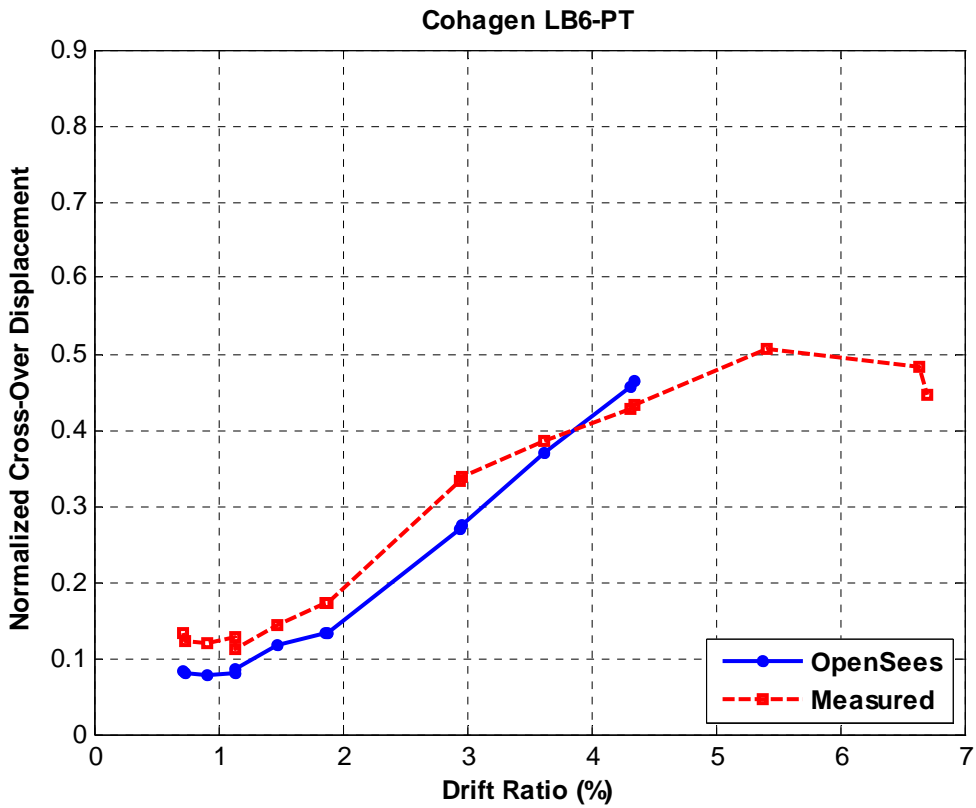


Figure B.15. Comparison of normalized cross-over displacement vs. peak drift ratio for Cohagen LB6-PT

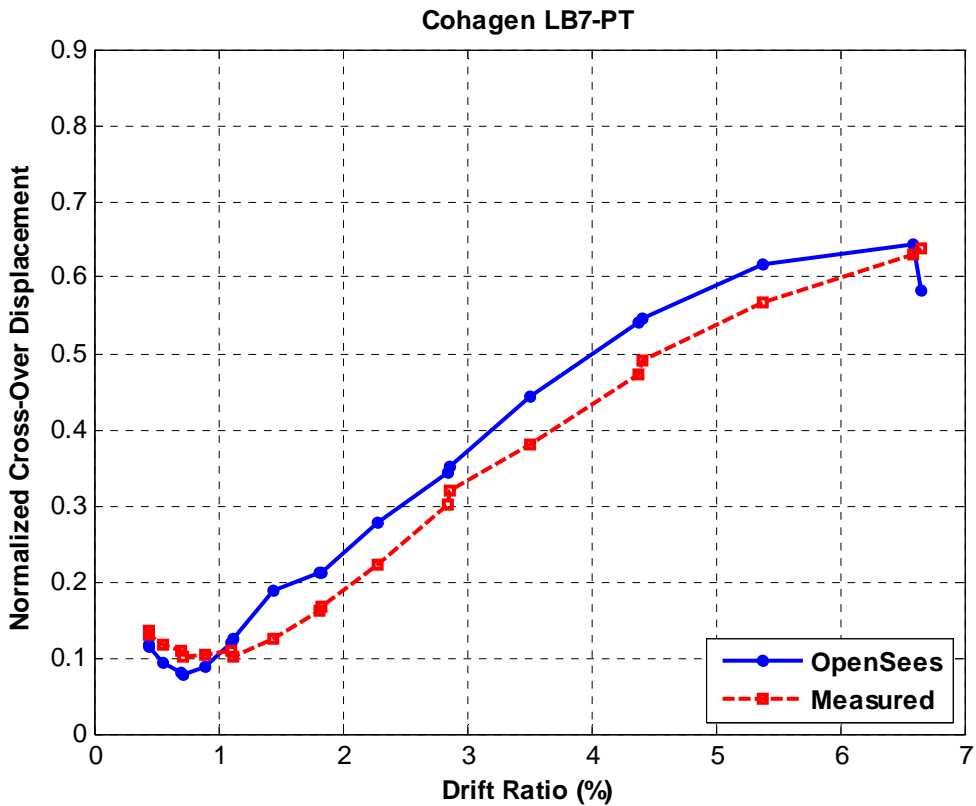


Figure B.16. Comparison of normalized cross-over displacement vs. peak drift ratio for Cohagen LB7-PT